NTNU Trondheim
Norwegian University of Science and Technology
Department of Marine Technology – Group of Marine Structures

MSC THESIS IN MARINE TECHNOLOGY

SPRING 2016

FOR

STUD.TECHN. Kristine B. Riste

Development of a Frequency-domain Model for Dynamic Analysis of the Floating Wind Turbine Concept - WindFloat

Background:
Coupled time-domain codes have been developed and now being widely used for design and analysis of offshore wind turbines. Due to strong couplings between wind-, wave-induced loads and responses, these time-domain codes are necessary for detailed design of floating wind turbines. While for preliminary design, long-term fatigue assessment and optimization, in which a large amount of analyses are normally required, it is still useful to develop computationally-efficient frequency-domain methods and models.

For structural design, member forces/moments or stresses under different wind and wave conditions need to be evaluated. Such analysis for a floating wind turbine typically involves prediction of external loads, dynamic analysis of motion and structural responses and detailed stress analysis. In order to derive a frequency-domain method, the analysis in each of the above steps needs to be linearized. Frequency-domain methods for integrated linear and second-order wave loads and responses have been developed and used for fatigue analysis of offshore oil and gas platforms. Such methods can still be applicable to floating wind turbines. The aerodynamic loads on the wind turbine rotor are in principle nonlinear. However, for a given mean wind speed and a small turbulence, frequency-domain models of aerodynamic loads on wind turbine blades have been developed for bottom-fixed offshore wind turbines considering turbulent wind fields. The integrated wind turbine loads (thrust, torque, etc., which will induce the floater motions) might be estimated using such linearized models. Motion analysis of floating structures is usually based on linear equations of motions, while fatigue stresses are typically obtained from linear structural analysis.

The purpose of this thesis is to develop a frequency-domain numerical model of the WindFloat concept with focus on hydrodynamic loads and responses. If time allows, the frequency-domain for integrated wind turbine loads based on the frequency-domain loads on blades should be developed and used for motion response analysis of the WindFloat.

The student will be provided with the design and numerical model of the WindFloat semi-submersible, the design and the characteristics of the NREL 5MW wind turbine and the frequency-domain model for distributed wind turbine aerodynamic loads.

Assignment:
The following tasks should be addressed in the thesis work:

1. Literature review on aerodynamic, hydrodynamic load and motion analysis of floating wind turbines, nonlinear features of the external loads, first- and second-order wave load analysis and stochastic linearization of equations of motions.

2. Study the design of the WindFloat concept. Build a numerical model in HydroD (considering both a panel model and a free surface model) and calculate the linear and quadratic transfer functions of the wave loads.

3. Based on the given WindFloat data, establish in the frequency domain the equations of motions. For a given wave spectrum, solve the equations of motions and obtain the motion response spectra (including linear or second-order responses).

4. Establish a time-domain model in Simo-Riflex-Aerodyn, perform dynamic response analysis and compare the obtained motion response spectra with the frequency-domain results. Discuss the discrepancy and the possible reasons.

5. Study the frequency-domain model of distributed wind turbine blade loads from Karl Merz and develop a frequency-domain model of integrated wind turbine loads for rigid-body motion analysis of the WindFloat in turbulent wind. If time allows, compare the motion response spectra obtained from the frequency-domain and the time-domain models.

6. Report and conclude on the investigation.

In the thesis the candidate shall present his personal contribution to the resolution of problem within the scope of the thesis work.

Theories and conclusions should be based on mathematical derivations and/or logic reasoning identifying the various steps in the deduction.

The candidate should utilize the existing possibilities for obtaining relevant literature.

The thesis should be organized in a rational manner to give a clear exposition of results, assessments, and conclusions. The text should be brief and to the point, with a clear language. Telegraphic language should be avoided.

The thesis shall contain the following elements: A text defining the scope, preface, list of contents, summary, main body of thesis, conclusions with recommendations for further work, list of symbols and acronyms, reference and (optional) appendices. All figures, tables and equations shall be numerated.

The supervisor may require that the candidate, in an early stage of the work, present a written plan for the completion of the work. The plan should include a budget for the use of computer and laboratory resources that will be charged to the department. Overruns shall be reported to the supervisor.

The original contribution of the candidate and material taken from other sources shall be clearly defined. Work from other sources shall be properly referenced using an acknowledged referencing system.

The thesis shall be submitted in two copies as well as an electronic copy on a CD:

- Signed by the candidate
- The text defining the scope included
- In bound volume(s)
- Drawings and/or computer prints which cannot be bound should be organized in a separate folder.

Zhen Gao
Karl Merz (Sintef Energi)
Supervisors

Deadline: 10.6.2016

Preface

This is a master thesis carried out during the spring semester of 2016, as a part of the study program Marine Technology at NTNU. The report presents a literature review on application of frequency domain methods for offshore wind turbines. Procedure for establishing a frequency domain method for motion analysis of the WindFloat concept. Comparison of the FD-model towards TD-model for the floating wind turbine subjected to wind and waves.

The assignment has been a great challenge and very interesting to work with. Unfortunately, there where problem with gaining the second order free surface in GeniE, that postponed the work on the state-space model. It was an aim to investigate more thoroughly on the motion caused by aerodynamic forces, but time is limited. Moreover, the simulation length of the wind-only simulations in SRA are at 2000 seconds, this is due to that the computer that was used is not capable of allocating enough space for TurbSim to generate longer time-series.

The readers should preferably have knowledge of basic hydrodynamics, fatigue assessment and dynamic analysis of offshore structures. The procedure is presented as carefully as possible, especially the aerodynamic part is thoroughly explained.

Trondheim, 10th June 2016

Kristine Bøyum Riste

Acknowledgement

This research is conducted as a final report in achieving a master thesis in marine technology at the Norwegian University of Science and Technology. The topic is selected based on the author's interest and skills. The assignment is built from supervisor Professor Zhen Gao's suggestions. A great thanks to Professor Zhen Gao for our bi-weekly meetings, more frequently mail-correspondence with resulting good guidance and interesting discussions. Gratitude also for advise from Karl Merz, for his publications on state-space model and for providing me with a model of the 5MW NREL turbine.

A great thanks for the wonderful co-workers at C1.076, for always being open for discussion, advise and a good laugh.

Thanks to Jon, for having a smile on his face and helping me out with computer issues and proofreading. And last but not least, to mom, dad and my sisters for unlimited support over the years at NTNU.

Abstract

In this master thesis a frequency domain method for dynamic response analysis of the floating wind turbine, WindFloat, has been established. The topic of response analysis in frequency domain is important for reducing computational time in preliminary design and fatigue calculations. The alternative approach with time-domain numerical methods are far more time consuming.

The main concern when establishing a frequency domain method, is that it requires a fully linear relationship between the load and response. Non-linear contributions in the dynamic equation of motion must therefore be linearised in a proper manner to reproduce the true response as correct as possible. The objective is to establish a frequency domain method for the WindFloat concept, and perform comparison to time-domain numerical methods.

The hydrodynamic model has been obtained by Wadam-analysis in HydroD, while the aerodynamic model was acquired by a state-space model.

Comparison of the results from the time-domain numerical method and the frequency domain method has been performed for three load-cases. The wind induced motions and wave induced motions have been examined separately. The results indicate that the non-linear contributions are of significance for both wind and wave-induced motions.

For the wind induced motions the comparison has only been applied for one simulation in SRA, while for the wave induced motions, averaging over ten simulations has been performed. Thus, the frequency domain method for wind induced motions is not properly validated and further investigation is recommended. The results indicate that the excitation in the low frequency domain is of significance, but that they are poorly represented in the range where the transfer functions have been extrapolated, for frequencies close to zero.

For the hydrodynamic model, the prediction of standard deviations and peak frequencies in the wave frequency range had less than 2.5% error for all of the loading conditions,

with exception of the extreme environmental condition. In the low frequency domain, the results had varying success, due to poor representation of the transfer function close to zero.

For further application of the hydrodynamic model it advised to either disregard the extrapolated solution, or more adequate, to implement values that can be interpolated. The wind-induced motions are highly dependent on the representation of the transfer functions to be correct. To get a better representation of the true behaviour, more work has to be performed on the aerodynamic model, both regarding validation, and correcting the transfer-functions.

Samandrag

I denne masteroppgåva er det etablert ein analyse for å berekne dynamisk respons i frekvensdomene på flytande vindturbinar. Berekningsmetoden i frekvensdomenet har vore etablert for separat undersøking av ytre krefter for bølgjeinduserte og vindinduserte rørsler. Dette emnet er viktig for å redusere kostnadar i tidleg design fase og utmattingsanalysar. Den alternative metoden, ved berekning i tidsdomene med numeriske metodar er mykje meir tidkrevjande.

Hovedutfordringa med å etablere ein metode for dynamisk responsanalyse i frekvensdomenet, er at det krev eit lineært forhold mellom last og respons på konstruksjonen. U-lineære effektar som er til stades i den dynamiske likevektslikninga må difor lineariserast slik at dei best mogleg representerer sann påkjenning som konstruksjonen vert utsett for. Føremålet med denne oppgåva er å etablere ein metode for kalkulering av dynamisk respons i frekvensdomenet for WindFloat.

Den hydrodynamiske modellen er oppnådd ved modellering i GeniE, for deretter å køyre Wadam-analyse i HydroD og for så og etterbehandle resultata i MATLAB. Den aerodynamiske modellen er oppnådd frå ein lineær state-space modell. Resultata vart verifisert ved å samanlikne dei med simuleringar utført i tidsdomenet i SIMO-RIFLEX-AeroDyn (SRA). Dette har vore utført for tre last-tilstandar. Resultata indikerer at det er viktig å ta høgde for dei u-lineære kreftene som er til stades for lav-frekvente rørsler.

For vindinduserte rørsler, har samanlikninga med SRA berre vore utført for ein simulering, medan snittet av resultata frå 10 simuleringar er samanlikna med løysinga i frekvensdomenet for bølgjeinduserte rørsler. Difor er ikkje resultata for vindindusert rørsle verifisert. Samanlikninga som er gjort gir berre ein indikasjon på kva ein kan forvente ved djupare etterforsking. Resultata syner at eksitasjonane i lavfrekvente område har betydeleg påverknad på rørslene, men dei syner dårleg samsvar med resultata frå SRA i område der verdiane i transferfunksjonane har vore ekstrapolert; i område for frekvensar nær 0.

For vidare bruk av denne metoden er det anbefalt å enten neglisjere verdiane som har vore ekstrapolert, eller implementere fleire datapunkt for låge frekvensar så det ikkje vert

naudsynt med ekstrapolering. Dei vindinduserte rørslene er særs avhengige av korrekt representasjon av transferfunksjonane i det lavfrekvente område. Difor må meir arbeid bli gjort på den aerodynamiske modellen, både med verifisering og med transferfunksjonane.

Contents

List of Figures

List of Tables

Nomenclature

Acronyms

BEM Blade element momentum

COG Centre of gravity

dof degree of freedom

FAST Fatigue, Aerodynamics, Structures and Turbulence (code)

FWT Floating wind turbine

FD Frequency domain

FE Finite element

GDW Generalized dynamic wake

JONSWAP Joint North Sea Wave Project

LF Low frequency

MBC Multi-blade coordinates

NREL National Renewable Energy Laboratory

NTM Normal Turbulence Model

pdf probability density function

QTF Quadratic Transfer Function

RAO Response amplitude operator

SRA SIMO-RIFLEX-AeroDyn (code)

SSWT Semi-submersible wind turbine

STAS State-Space

STD Standard deviation

TD Time domain

WAFO Wave Analysis for Fatigue and Oceanography (MATLAB toolbox)

WAMIT Wave Analysis at MIT (code)

WF Wave-frequency

WT Wind turbine

Latin Characters

A Added mass matrix / matrix connected to states in state space-model

B Damping matrix / matrix connected to inputs in state-space model

C Restoring matrix / matrix connected to states in state-space model

$\mathbf{C}_A$ Added mass coefficient matrix [3x3]

$\bar{c}$ generalized damping

D significant length / matrix connected to inputs in state-space model

f frequency 1/s

f_1 Linear hydrodynamic force, expressed in time domain

F_1 Linear hydrodynamic force, expressed in frequency domain

f_2 Second order hydrodynamic force, expressed in time domain

F_2 Second order hydrodynamic force, expressed in frequency domain

$\bar{f}$ generalized external force

F External force vector

$\mathbf{f}_b$ Fluctuating buoyancy force calculated in a coordinate system fixed with the Morison model

$\mathbf{f}_c$ Fluctuating hydrostatic restoring force representing the first order restoring contributions integrated in the equation of motion.

$\mathbf{f}_g$ Fluctuating gravity force representing the acceleration of gravity calculated in a coordinate system fixed with the Morison model

Fx Thrust force

g Gravity constant

$\mathbf{H}_{FY}$ Transfer function for relation between force and displacement

H_s significant waveheight

$\mathbf{H}_{UF}$ Transfer function for relation between force from wind and wind speed

H_1 Linear transfer function for hydrodynamic loads

h_1 Linear impulse response function for hydrodynamic loads

H_2 quadratic transfer function for hydrodynamic loads

h_2 quadratic impulse response function for hydrodynamic loads

I Identity matrix [3x3]

k wave number

$\bar{k}$ Generalized stiffness

L Identity matrix in state-space model

L_K Integral scale parameter in Kaimal Spectrum

M tower base bending moment

M Mass matrix

$\bar{m}$ Generalized mass

Mx Torque

n normal-vector.

p Pressure

R_{kk} Autocorrelation function for a stochastic process. Subscript kk denotes which stochastic variable.

Rn Reynolds number

S_F^{wind} one-sided power spectra for wind force

$S_K(\omega)$ Kaimal Wind Spectrum

S_M power spectra for tower base bending moment

S_U one-sided power spectra for wind speed

T Thrust force

t time

T_p Peak period

u input vector in STAS

U Wind speed

$\bar{U}_{hub}$ mean wind speed at hub height

V_M Displaced volume of Morison element.

x States vector in STAS.

$\ddot{x}$ local body acceleration

$\dot{x}$ local body velocity

x local body displacement

y output vector in STAS

$\ddot{\mathbf{Y}}$ Structure acceleration vector

$\dot{\mathbf{Y}}$ Structure velocity vector

Y Structure displacement vector

Z Surface elevation in frequency domain

z coordinate.

Greek Characters

α coefficient for wind-speed profile

α_U coefficient for the pdf of wind speed.

β_U coefficient for the pdf of wind speed.

$\alpha_H C$ coefficient for the joint pdf of significant waveheight for a given wind speed.

$\beta_H C$ coefficient for the joint pdf of significant waveheight for a given wind speed.

Δ Notation for discrete interval.

λ Tip speed ratio

λ_r Local tip speed ratio

μ mean value

μ_{LTC} mean value for joint pdf for wave period for a given significant wave height.

ν Kinematic viscosity

ρ density

Σ Summation notation.

σ Standard deviation (STD)

σ_{LTC} STD for joint pdf for wave period for a given significant wave height.

σ_K STD of the Kaimal spectrum

θ random phase angle

ϕ, Φ velocity potential.

ω Frequency or angular velocity of flow

ζ Instantaneous surface elevation in time domain

Other

∇ The nabla operator $\hat{i}\frac{\partial}{\partial x} + \hat{j}\frac{\partial}{\partial y} + \hat{k}\frac{\partial}{\partial z}$, a differential operator.

Commonly Used Expressions

Axial induction factor: A measure for the rate of change of the velocity in the upwind area close to the rotor.

Rated wind speed: Characteristic value for the wind turbine, describes the wind speed at which the torque reaches its maximum value, for above rated wind speed, the torque has this constant value due to the pitching of the blades. For below rated wind speed, the thrust force and the torque is increasing up to rated wind speed, there is no pitching of the blades. And for above rated wind speed the thrust force decreases, hence thrust force has its maximum at rated wind speed.

Thrust force: The horizontal force on the rotor.

Torque: The moment about the horizontal axis of the rotor.

hub height: Distance from bottom of tower to the hub of the turbine. (Where the hub is in the centre of the blades)

Pitch: rotation about a y-axis

Yaw: rotation about a z-axis

Roll: rotation about a x-axis

Surge: translation along x-axis

Sway: translation along y-axis

Heave: translation along z-axis

Eigenmode: Description of a displacement pattern that a structural member has due to vibration in a certain frequency.

Spectrum: General a description of which frequencies that are present and how much energy they excite. Spectra are used, e.g. to describe a sea-state, where the peak frequency will show which frequency that contains most energy. From spectrum it is possible to derive time-series for e.g. sea-states that has properties of that spectrum.

Chapter 1

Introduction

This is the report of a master thesis executed at NTNU during the spring semester of 2016. The main topic of the thesis is to establish a frequency-domain method for dynamic response analysis for a floating wind turbine. This topic was also reviewed in a project thesis performed during the autumn semester of 2015. Therefore the work presented here was to some extent performed during the project thesis. This chapter will introduce the background to why this topic is of interest in Section 1.1. A literature review has been conducted in order to gain knowledge in the field of study, a summary is presented in 1.2. The objective of the master thesis is presented in Section 1.3, and finally the structure of the report in Section 1.4.

1.1 Background

The market for renewable energy is increasing. As there is no doubt that the resources of fossil energy sources are limited, the need for alternative energy sources are inevitable. Land based wind turbines have been used for decades, but the concept on offshore windfarms is fairly new. Bottom fixed wind turbines has been deployed with success in several sites in Europe, but it is now of interest to see how floating structures will work in deep water depths far from shore. Statoil recently got permission to deploy their Hywind concept

outside the coast of Scotland (ref. Nilsen [2015]). Hywind is a floating spar buoy moored to the seabed. Ros and Costa [2015] discuss several challenges that has to be solved in order to have success with offshore wind-farms. Among others, advanced simulation tools is one of them, and a problem here is especially the lack of data from full-scale testing to verify the calculations. According to Bachynski et al. [2015] there is a problem with scaling wind and waves simultaneously. Waves are scaled by Froude number while wind is scaled by Reynolds number. Model-testing of wind turbines has been done by applying wind and wave, but the different scaling effects make it difficult to get an accurate enough result. Thus, a different approach for model-testing were performed during the autumn of 2015, Bachynski et al. [2015] performed model tests in the ocean basin at Marinteknisk Senter in cooperation with MARINTEK and NOWITECH by applying forces on a frame that should simulate the rotor on a wind turbine. This was done by advanced programming in real time, calculating the loads that should be applied to the frame while the waves were generated to excite the hydrodynamic loads on the structure.

When considering the Norwegian coastline, even short distances from the shore tend to have water depths that are too large for the bottom fixed concepts for offshore wind turbines that has been developed so far. According to Midling [2015] the Norwegian coastline is not suited for the bottom-fixed concepts. Nevertheless cost is an important factor, and the price for extracting energy from the wind should be competitive to the cost of other energy sources. In Midling [2015], John Olav Gjæver Tande, the director of NOWITECH, claims that the technology development for offshore wind farms is still in its initial phase, and that there is great potential for cost reduction. An efficient way to calculate the loads on offshore wind turbines can be one of the solutions that will reduce the costs in design and verification of wind-power plants.

Development of competitive renewable energy solutions will be important for future energy demand. Li et al. [2015] has investigated the available power for different sites across Europe, power from wind and wave that can be used for combined energy devices. This research can also be important to be able to calculate both extreme loads and fatigue life for an offshore floater. With today's computer technology, calculating fatigue damage in time

domain on offshore structures is highly costly. With a look at the broader view, offshore semi-submersible platforms, there has been developed a recognized method in order to calculate the fatigue life in frequency domain (DNV [2012]). Therefore it is desirable to establish a frequency domain method for calculating the loads on a semi-submersible wind turbine (SSWT).

The procedure is not straight forward, if you compare it to the semi-submersible platform one of the challenges with the SSWT is that you have greater coupling effects between wind and wave. When performing fatigue analysis for structure subjected to waves it is only necessary two have two environmental variables; wave period and significant wave height, but for floating wind turbines (FWTs) one must also consider mean wind speed as a variable. In this thesis a 5MW NREL wind turbine is considered, on a modified WindFloat design. Currently (January 2016) there is a 2.3MW WindFloat prototype concept being tested outside the coast of Portugal. It has been deployed in the Atlantic Ocean since 2011 and can provide valuable information on full-scale data for FWTs. A second generation of the WindFloat design has been engineered to a reduction in cost of 60% per MW in comparison to the prototype that was deployed in 2011 (from Snieckus [2015]). This example demonstrates what great cost reductions that are possible to obtain in the industry for offshore wind.

Kvittem and Moan [2015] has performed fatigue analysis in time domain for the modified WindFloat design. The non-linear contributions they had to take into account was the catenary mooring line forces, viscous and aerodynamic forces and in addition to include load calculation at updated position due to large displacements. To get an idea of the magnitude of these simulations, for this design, the results showed that it would be necessary with 3-6 hour simulations in order to capture the slowly varying responses. This is due to the long natural periods for this structure, with a natural period in surge at approximately 100 seconds (ref. Kvittem et al. [2012]). In addition considerations on what bin-size the different variables should have are important, and how many load cases one must account for in a fatigue assessment. Kvittem and Moan [2015] also studied the effects of misaligned wind and wave, and concluded that aligned wind and wave gave the highest

fatigue loads. This can influence the number of load cases, as it implies that it is a conservative assumption to only include the aligned wind and wave. It is however important to be careful as the wave direction is the variable that determines which structural part that experiences the most fatigue damage.

Frequency domain methods for calculating the loads on offshore wind turbines has previously been developed by Van Der Tempel [2006] for a bottom fixed turbine, and by Kvittem and Moan [2014] for the modified Windfloat. Wayman et al. [2006] developed a frequency domain method for coupled dynamic modelling of a MIT/NREL shallow Drafted Barge and a MIT/NREL Tension Leg Platform. This was done by applying FAST code to achieve the aerodynamic and structural dynamic of the structures, and WAMIT code for wave load and response simulation tool. There was no comparison to time domain simulation in the report by Wayman et al. [2006], but Bachynski and Moan [2012] applied a frequency domain method on different TLP designs and made comparisons with time domain simulations. In that paper the results showed that the frequency domain method could capture the wave response in low sea states with acceptable accuracy, but that for severe sea states it did not compute sufficient solutions. The wind was poorly represented, and was found to be of important significance, so further work on the concept was revised. Van Der Tempel [2006] also achieved good results for fatigue calculation in frequency domain compared to time domain. The design investigated was a bottom fixed monopile, and so it was possible to assume independent wave and wind induced stress. Fixed structures has smaller motions excited by external forces compared to a floating moored structure, therefore this assumption is valid and simple superposition could be applied.

One of the issues that has to be dealt with when solving the Equation of motion in frequency domain is that it is necessary to linearise the forces. When the forces are linearised the solution will lose some of the excitations that non-linear forces contribute to. Thus, it is important to compare the solutions achieved in the frequency domain with solutions from time domain procedures. Then it is possible to identify for which frequencies it is difficult to obtain the correct response, and the linearised components can be altered to take into account some of these excitations. For fatigue damage, well established frequency

domain methods are used because the importance of the results is the entire life cycle of the structure and the estimated stress ranges it is subjected to. Extreme responses that occurs rarely, has little impact on the fatigue life. Consequently, in order to calculate the fatigue damage it is often used some conservative assumptions to decrease the probability of failure.

1.2 Literature Review

In the following section a summary of the literature review is described in detail. First discussion on the environmental conditions for where the SSWT will be situated is explained in Section 1.2.1. Here the methods for achieving these data are explained. Then follows Section 1.2.2, describing the validity of superposition of fatigue loading, based on Chapter 7 in the dissertation by Kühn [2001]. Then follows a summary of the frequency domain method, which is presented in Section 1.2.3, this is based on work by Kvittem and Moan [2014] on the modified WindFloat. An approach to include turbulence and dynamic stall in a frequency domain method for wind turbines are presented in Section 1.2.4, based on the work presented in Merz et al. [2012].

1.2.1 Environmental Conditions

Li et al. [2015] have investigated environmental conditions for joint wind and wave distribution at different European sites. The distributions are achieved by collecting Hindcast data and fitting analytical distributions for these. In this way distributions are suggested for the wind and wave conditions at these sites, in addition to providing distributions for calculating fatigue life, as well as extreme loads for probability of exceedense of 50 years. The site of the semi submersible offshore wind turbine investigated in this project will be situated in the North Sea outside the coast of Norway. Where the water-depth is 202 meters and the environmental loads estimated by Li et al. [2015] are as presented in Table 1.1.

When designing a floating device it is important to look at the loads due to the waves. For the North sea, JONSWAP-spectrum are most often used to express the harsh weather conditions. JONSWAP-spectrum are derived from the more known Pierson-Moskowitz spectrum, but the distribution is more narrow-banded, based on the lambda parameter. This means that more energy is concentrated in the area close to the peak frequency.

The statistics from the site outside the Norwegian coast that Li et al. [2015] achieved are presented in Table 1.1. This gives a brief representation to the expected loads that the SSWT must be designed for. Average wind power density gives an indication of how much power it will be possible to produce at the site. The average wave power density is presented since this paper discussed wave-energy devices as well, but it can also indicate the hydrodynamic loads on the structure. The 50-year design values show the extreme conditions that can be expected.

Table 1.1: Estimated environmental conditions for North sea in site *Norway5* from Li et al. [2015].

Description	**size**	**unit**
Water depth	202	[m]
Average wind power density at 80m	1094.84	[W/m^2]
Average wave power density	46.43	[kW/m]
50-year U_w at 10m	33.49	[m/s]
50-year H_s	10.96	[m]
Mean value of T_p	11.06	[s]

By a comparison of the 18 sites that are evaluated in Li et al. [2015] the site presented in Table 1.1 had the maximum values for the 50-year wind speed and significant wave height, and had the second highest expected value for average wind and wave power density.

1.2.2 Superposition of Fatigue Loading

The principle of using superposition to solve dynamic problems yield that it is possible to divide the problem into several parts and achieve the complete solution by adding together the solutions from the different independent parts of the problem. A good example

is how the hydrodynamic problems on floating devices are divided into a radiation problem and a diffraction problem, providing a superimposed solution of the simultaneous response. Fatigue damage must often be considered early in the design development, and therefore it is of interest to have an efficient method to calculate these. The following section is based on Chapter 7 of Kühn [2001].

Kühn [2001] discuss how to properly separate the simultaneous response and how to apply superposition to achieve a solution of the simultaneous response. When establishing a solution for the equation of motion for a FWT it is important to consider the coupled wind and wave interactions of the structure. The studies show that wind and waves are somewhat independent, which means that not much of the waves generated are due to wind. This assumption can be justified when assuming stationary short term environmental states.

When simplifying a complex problem one of the most sensitive contributions are the damping terms. Some damping has non-linear behaviour and is in general difficult to achieve a good estimation of. For a floating wind turbine both hydrodynamic and aerodynamic damping must be considered. The studies reveals that the aerodynamic damping of the fore-aft motion of the wind turbine is essential to capture in order to achieve a reasonable result, thus it is of great importance to have a good estimate for the damping terms.

Kühn [2001] has applied an example of a bottom fixed monopile with a 3MW wind turbine. For this concept it is valid to assume that the motions of the submerged part of the structure is smaller than the water particles, so that viscous damping and radiation damping are small compared to the structural damping. However for a floating wind turbine this assumption will most likely not be valid.

The drag forces are contributing to hydrodynamic damping, this is especially of interest for slender structural members. For the WindFloat concept this would relate to the braces and mooring lines where you have strong interaction with the hydrodynamic forces and structural kinematics. This yields that separating the external force and response must be carried out with great care.

In order to estimate the aerodynamic damping of the fore-aft translation of the wind turbine Kühn [2001] evaluates the following three different approaches which will be briefly explained.

1: Closed form linearisation

2: Numerical linearisation

3: Non-linear time domain simulation

The first method is simple and gives a physical insight to the solution. It can be established by simple blade/element momentum theory (BEM), or by most aerodynamic code. By assumption of that the upper bound for attached flow is described by the slope of the lift coefficient. The second method requires more extensive aerodynamics, includes unsteady effects. Hence, a system with large number of degrees of freedom must be solved in order to obtain a solution. The third method considers simulations of steady state response under harmonic excitation and decay tests of the free vibrations. The contribution from the latter is straight forward, but for the harmonic excitation the stochastic vibration of the response must be filtered out in order to obtain a solution. Kühn [2001] concluded that all methods gave similar results, but it is important to keep in mind that this has only been evaluated for the design concept of a bottom fixed monopile.

The topic of superposition of fatigue loading for an offshore wind turbine is advanced. The objective is to replace method of using time-domain simulations and rainflow-counting approach to achieve the stress cycles. Kühn [2001] performed a literature review on the topic, and it was difficult to achieve any methods sophisticated enough to be applicable for the combined wind and wave response of a wind turbine. One of the great obstacles is that several methods are assuming two independent narrow-banded Gaussian processes, which yields a conservative assumption since the wind distribution is broad banded while waves are narrow-banded. To completely separate the fatigue loading into wind and wave contributions would according to Kühn [2001] give too conservative results. The dynamic problem that was considered to be most similar to the floating wind turbine is coupled mooring loads, where both the eigenmodes of the vessel and the eigenmodes of the mooring lines had to be taken into account.

For fatigue assessment of a floating wind turbine the S-N approach is most relevant to use. The most desired method to evaluate was a combination of damage equivalent fatigue loads for two stationary random processes. The concept of damage equivalent fatigue loads is basically to have an expression that can compute an equivalent stress-range that can be directly inserted into a S-N curve to find the equivalent fatigue damage. Achieving this expression is not straight forward, Kühn [2001] decided to use a method referred to as "weighted quadratic superposition of equivalent stress ranges". In short terms, this method calculate an equivalent stress range for two responses, and weight the response based on the ratio between zero-crossing periods of the separate response divided by the combined response. The combined response is unknown and therefore substituted by spectral moments. A root of this ratio is used for weighting the separate damage loads to achieve the weighted equivalent stress range. In addition, a direct quadratic superposition of equivalent stress ranges were proposed, but not recommended. This approach makes it necessary to assume that the zero-crossing period for the wind and wave are equal, which in general is not true. In order to achieve these spectral parameters an assumption on which spectrum to be used has to be made. For wind, examples of these are Kaimal spectrum and Von Karman, for waves Pierson-Moskowitz and JONSWAP are two possibilities. The two methods mentioned above gave non-conservative results for larger bandwidths, the weighted quadratic superposition of equivalent stresses gave larger errors than direct superposition of equivalent stresses, but these were positive, thus more conservative. To verify the methods Kühn compared the results with time-domain analysis, the results experienced some errors, but gave sufficient accuracy for a simplified approach. The difference between the two methods were not large, most likely due to the errors in estimating the zero-crossing frequency causing proceeding errors in the weighted method. Therefore, Kühn [2001] recommended use of the simpler direct method.

1.2.3 Frequency Domain Method

The frequency domain method is a powerful tool to use for calculating the dynamic response, it must however be established with great care as the frequency domain method

is a linear solution to the equation of motion, which is meant to solve a non-linear problem. This section will briefly elaborate the work done by Kvittem and Moan [2014] on how to establish a frequency domain method for the WindFloat design concept, and discuss some of the results that were achieved and their applicability.

The governing equation is the linear equation of motion (Equation 1.1), which describes the motion of the wind turbine for six degrees of freedom due to loading from external forces.

$$(\mathbf{M}+\mathbf{A}(\omega))\ddot{\mathbf{Y}}(\omega)+\mathbf{B}(\omega)\dot{\mathbf{Y}}(\omega)+\mathbf{C}\mathbf{Y}(\omega)=\mathbf{F}(\omega) \tag{1.1}$$

The external force and the platform motions can be described by complex transfer functions dependent on frequency. These give a relation between e.g. platform motion and wave elevation. In the same manner a complex transfer function describing the relationship between the external force and the platform motions as shown in Equation 1.2 can be obtained. Hence, Kvittem and Moan [2014] has separated the simultaneous response due to wind and wave.

$$\mathbf{Y}(\omega)=\mathbf{H}_{FY}(\omega)\mathbf{F}(\omega) \tag{1.2}$$

By use of transfer functions the variance spectra for force due to wind can be obtained by Equation 1.3. By knowing the wind-spectrum and the transfer-function. Wind spectra can be for example Kaimal-spectra. The study by Kvittem and Moan [2014] have used the variance spectra of the rotor forces to obtain the external force from the wind. To get as correct representation as possible, the wind speed in the function is the relative wind speed experienced by the rotor. The relative wind speed is, among other things, dependent on angle of attack, which influences the drag and lift coefficients. Consequently it has direct influence on the rotor forces.

$$S_F^{wind}(\bar{\omega})=|H_{UF}(\bar{\omega})|^2 S_U(\bar{\omega}) \tag{1.3}$$

Where the subscript denotes relation, for this case, the force, F, due to wind-speed, U. All

terms are complex, harmonic motion is described by an amplitude and $e^{i\omega t}$.

The presence of the rotor has a damping effect in both wave induced motions and wind induced motions, that must be linearised. Regarding damping, another coupling effect was observed by Kvittem and Moan [2014], this was that for low frequencies, presence of motions due to waves has a damping effect on the motions induced by the wind. Kvittem and Moan [2014] stated that the source of this phenomena is most likely due to second order terms, where both the velocity of the waves and the wind is involved in the thrust force. This phenomena is not modelled by the frequency domain method established in Kvittem and Moan [2014].

The method requires linearisation of quadratic damping terms (present in **B**-matrix in Equation 1.1). For this concept, platform motion amplitudes were used to linearise both wind and wave induced motion. The aerodynamic damping is represented by the change in thrust force as a function of wind speed. This was done by Bachynski [2014], where the procedure was to consider the turbine fixed, then apply constant wind, keep the pitching of the blades for that wind-speed fixed, and apply wind 0.25 m/s above and below the initial wind configuration. This was done for a range of wind speed from approximately 5 m/s to 25 m/s, and based on the change in thrust for each of these intervals the aerodynamic damping could be achieved as a function of wind speed. It was calculated for surge, heave and pitch degree of freedom, and the results showed a damping ratio of 4-5 % for all the wind-speeds that were tested.

When applying a frequency domain method it is important to consider the eigenmodes of the system. Previous studies by Kvittem and Moan [2015] has shown that the significant excitation comes from the first bending mode of the turbine, therefore, higher order modes were neglected. The eigenmodes can usually be obtained easily by using finite element software, but for this design that is problematic. The reason for this is that the design needs to take into account both the flexibility of the structure, as well as the flexibility of the support. For flexible systems use of superposition will not give the correct eigenmodes. However the mode shape of the first bending mode had to be achieved, the procedure proposed by Kvittem and Moan [2014] to solve this problem is as follows. The

system is simplified to a single degree of freedom with generalized properties. Aerodynamic damping is simplified as a damping term in the top of the tower. Lumped mass properties are applied in the top of the tower, containing the mass of the hub and nacelle. In the tower bottom a rotational spring is applied, accounting for the damping in pitch motion. The inertia forces from the foundation mass and added mass are applied in the node. With this generalized system (As described by Equation 1.4) decay analysis of the tower top deflection was performed by time domain simulations. The time-series were then filtered to include only the frequencies fluctuating about the first bending moment of the tower. Finally third order spline interpolation was used to get 1st and 2nd derivatives of the modeshapes.

$$\bar{m}\ddot{x}(t) + \bar{c}\dot{x}(t) + \bar{k}x(t) = \bar{f}(t) \tag{1.4}$$

Since it is not possible to get an exact solution for the eigenmodes with respect to both the flexibility of the structure and the support, the procedure was also performed on a fixed turbine where the results could be compared to an exact solution. The results showed that the eigenfrequency obtained by using generalized coordinates were close to the true eigenfrequency, which increase the credibility that the eigenfrequency for the entire system can be a good estimation with this procedure.

For the fatigue assessment the timeseries for the tower base bending moment were generated by Equation 1.5. Where S_M denotes the spectrum for the bending moment and θ is a random phase.

$$M(t) = \Sigma_{k=1}^{N} \sqrt{2S_M(\omega_k)\Delta\omega} cos(\omega_k + \theta_k) \tag{1.5}$$

The solutions has been calculated for four different cases, three frequency domain methods have been applied. First one, considers a rigid structure subjected to wind and wave, second include the first fore-aft bending mode, and is subjected to wind and wave, while the third include the first fore-aft bending mode, but is only subjected to wind. These

methods are compared towards full time-domain analysis in SIMO-RIFLEX-AeroDyn(SRA). In order to compare the results standard deviations of the motions, the tower base bending moments and variance spectra of the moments are presented in graphs.

The results revealed that the prediction of the bending moment was good for wind and wave-only simulations, and combined wind and wave. Although the FD-method was not able to represent the motions due to wind accurately, the results were satisfying, which indicates that the motions were dominated by forces excited by the rotor and the blade passing frequency. By including the generalized approximations for excitations due to blade-passing frequency and dynamic amplification from waves the results improved. The amplitudes of the tower bending moment were underestimated for every case, so although the standard deviation had an error of less than 6 % in all cases, the fatigue damage calculations showed significant errors. This is due to that in fatigue damage the stress range is proportional to a power coefficient of 3 or 5 (dependent on the magnitude of the stress range). Further work on the method was therefore revised.

1.2.4 Dynamic Stall and Turbulence in Frequency Domain Calculations for Wind Turbines

Merz et al. [2012] has investigated how to establish a frequency domain method for calculating fatigue loads on a stall-regulated wind turbine. In Merz et al. [2012] only one blade is considered. The outline of the method in Merz et al. [2012] will be presented in this section. One of the important effects that are included in this FD-method is that both the tangential in-plane component of turbulence and dynamic stall is included. This accounts for the time delay to the movement of the separation point on the airfoil as the angle of attack fluctuates about a mean.

First, a description on how Merz et al. [2012] accounts for the tangential turbulence components. A spectral description of turbulent velocity fluctuations are described for three degrees of freedom, the turbulence is rotationally sampled, which implies that the frame is rotating with the same rotational speed as the wind turbine. In order to simplify the prob-

lem, an assumption of isotropic and homogeneous turbulence is applied. That coincides with Taylor's frozen turbulence hypothesis.

For statistical calculations one can separate the contributions in two categories, stochastic (random) contributions and deterministic (dependent) contributions. For this purpose the turbulence in the wind is a stochastic process, while tower shadow and wind shear has deterministic dependence on the stochastic process. The deterministic loads are represented by Fourier series, including the multiples of the rotational frequency of the turbine (1P, 3P etc. for a 3-bladed turbine). In Merz et al. [2012] the method is intended for use in preliminary design, therefore phase is neglected, and the deterministic loads are accounted for by adding spikes in the spectrum that represents the axial velocity. The spikes are added by including the coefficients that were obtained in the Fourier Series.

Now a brief description on how Merz et al. [2012] has included the effects of dynamic stall will be presented. A sum of harmonic terms is used to represent the stochastic excitation due to turbulence in the wind. The blade is considered stationary and then harmonic excitation is applied. The aim is to account for the change in the lift coefficient due to a fluctuating angle of attack at the blade. With a quasi-static representation of the lift coefficient towards angle of attack inaccurate results are obtained due to that the true dynamic behaviour of the separation point is fluctuating.

The excitations are caused by fluctuations in the velocity that are present due to turbulence, whilst damping is caused by fluctuations in the velocity due to the vibration of the blade. For harmonic excitation the phase is irrelevant since it is not a part of the spectral density, but the blade respond to the harmonic components which yields that the response is dependent on aerodynamic damping.

The dynamic stall model is described by slopes in lift force versus angle of attack. Two equivalent slopes are necessary for computation, one representing the excitation force and one describing the aerodynamic damping. Merz et al. [2012] has used the Øye model, which interpolates the lift coefficient between two extreme values. These are represented by one situation where you have fully attached flow at the airfoil, and one where the blade experiences fully separated flow. Thus, laminar and turbulent flow respectively. The equi-

valent slopes can then be introduced in a transfer function to get a linear relation between the velocity spectra and the force spectra. The equivalent slope to calculate the response for blade excitation is obtained by constructing a frame for the limits of the hysteresis loop (dynamic fluctuation) at a given angle of attack, the diagonal of this rectangle is then the equivalent slope. In order to get the equivalent response for damping, the dissipated energy of one blade rotation is calculated at each section of the airfoil from root to tip. By studying the fluctuations in the lift force over one cycle the equivalent damping slope is obtained.

This approach has been compared to non-linear time domain simulations in order to verify the linearisation. To sum up, the linear method gives a conservative result when the damping is close to zero or negative, however the method shows significant improvement compared to when dynamic stall is not included and only the quasi-static linearisation of the lift coefficients are used. Significant error is also reported when the damping ratio is close to zero. The results showed that the contribution from the dynamic stall derivations were most significant for low wind speeds and around rated wind speed, where the quasi-static 2D coefficients overestimated and underestimated the damping respectively. The error compared to TD-simulations are greatest when the airfoil stalls in a short time interval. If the airfoil is more smoothly stalled the errors are large for small frequencies and large amplitudes. The method is however reasonably accurate in the range where blades typically are experiencing vibration, hence, when the amplitude of fluctuation in angle of attack is small. The results are in general conservative as the damping obtained from the linearised method is smaller than what the non-linear calculations implies.

1.3 Objective

The objective is to develop a frequency domain method for dynamic response analysis of WindFloat. The stepwise method to reach this aim is listed below.

1. Conduct a literature review on aerodynamic and hydrodynamic response analysis of floating wind turbines. Nonlinear features of the external loads shall be included.
2. Develop numerical model of WindFloat in HydroD that is capable of calculating both linear and quadratic transfer functions representing the relation between force and motion for wave loads.
3. Establish the dynamic equation of motion in the frequency domain for WindFloat. For given wave spectra, present the motion response spectra.
4. Establish a time-domain numerical model in SIMO-RIFLEX-AeroDyn and perform dynamic response analysis for the same wave-conditions as the frequency-domain method is solved for. Then compare the motion response spectra from time-domain with the frequency-domain solution.
5. Study the state-space model in frequency domain for loads on wind turbine blades from Karl Merz. Develop a model for integrating the distributed loads to thrust force and application for global analysis of rigid-body motion on WindFloat. If time allows, compare motion response spectra obtained from the frequency-domain and time-domain models.

1.4 Structure of the Report

The report is structured as follows:

Ch.1 Gives an introduction to the background of the study, followed by a literature review closing in on the motivation for examining the objectives.

Ch. 2 Describes the theory behind dynamic response analysis for both hydrodynamic and aerodynamic application. The chapter differs between the hydrodynamic and aerodynamic part.

Ch. 3 Contains a step by step procedure on how to reach the scope of the thesis. Introduction to the design applied for dynamic response analysis is given, along with the criteria for setting the environmental condition. Following are the key aspects about the modelling of the hydrodynamic and aerodynamic model. Relevant assumptions and simplifications from Chapter 2 are elaborated, with an outline on the postprocessing of the results. In addition, a brief explanation of the theory behind SIMO-RIFLEX-AeroDyn is presented along with the configuration for the different simulations.

Ch. 4 The results are presented.

Ch. 5 Discussion of the results.

Ch. 6 Conclusion of the report.

Ch. 7 Recommendations for future work are presented.

Chapter 2

Methodology

This chapter will present the methodology that fund the basis for the theory necessary to apply in order to conclude the objectives. The overall aim is to establish a frequency domain method which is able to calculate the load and response of SSWT, WindFloat. Several aspects has to be considered, the FWT will be subjected to external forces from both wind and waves. These may have some coupling effects that affects the response, but the total solution for the response will be obtained by using superposition, by separating the response due to wave and wind. From potential flow theory the governing equation for the linear equation of motion (Equation 2.1) can be obtained. This equation funds the basis for establishing the frequency domain method. Here $\mathbf{Y}$ is a vector, representing the global displacement in six degrees of freedom, and its derivatives are the velocity and acceleration. The degrees of freedom are three translations, surge, sway and heave, which are motions in global x, y and z-direction respectively. In addition there are three rotations; roll, pitch and yaw, that represent the rotations about x, y and z respectively. The mass and restoring matrix are constant, while added mass, damping and the external force are frequency dependent.

$$(\mathbf{M}+\mathbf{A}(\omega))\ddot{\mathbf{Y}}(\omega)+\mathbf{B}(\omega)\dot{\mathbf{Y}}(\omega)+\mathbf{C}\mathbf{Y}(\omega)=\mathbf{F}(\omega) \tag{2.1}$$

In Equation 2.1, the problem is decoupled into hydrodynamic and aerodynamic external

forces on the right-hand side. Allowing for separate considerations, when calculating these forces, so that the complete solution for simultaneous response can be superposed. How the global motions of the platform and the hydrodynamic external forces are obtained, are presented in Section 2.1. Then the theoretical background on how to capture the external forces from wind is presented in Section 2.2. A closer look at the differences between applying wind in the frequency-domain and the time-domain are presented in Section 2.3. Then finally, the equations for gathering the contributions from wind and waves and presenting the complete motion spectra are presented in Section 2.4.

2.1 Establishing FD-method for Hydrodynamic Loads

This section is divided into three parts. The boundary value problem is presented in Section 2.2.1. Following, is the theoretical background on how to obtain the dynamic equation of motion (2.1.2). And finally, how to go from TD to FD, and how to obtain spectral formulations for the loads and motions are elaborated in Section 2.1.3.

In order to establish the terms in Equation 2.1, it is necessary to define some boundary conditions and governing equations for the structure and its surrounding fluid domain.

First a domain where the equations must be satisfied is defined. Consider the floating structure, then the fluid domain is restricted by the free surface, the seabed, the surface of the structure and vertical planes intersecting the surface and structure infinitely far away from the structure in each direction. Within this volume, two governing equations must be held, conservation of fluid mass, and conservation of fluid momentum. The former equation yields that the mass in the fluid domain is constant and the latter states that Newton's second law must be held.

2.1.1 Boundary Value Problem

The formulas presented to describe the boundary value problem are collected from ch.2 in Faltinsen [1993]. Assumptions that are necessary to apply in potential flow theory, is that the water is incompressible, inviscid and irrotational. These assumptions are implied in the governing equation of the boundary value problem, as stated in Equation 2.2.

$$\nabla^2\Phi = 0 \tag{2.2}$$

The velocity potential is used to describe the linear and quadratic dynamic pressure in Bernoulli's equation for obtaining the pressure.

$$p + \rho g z + \rho\frac{\partial\phi}{\partial t} + \frac{\rho}{2}|\nabla\phi|^2 = constant \tag{2.3}$$

In order to obtain an expression for the velocity potential, boundary conditions in the fluid domain must be described. The kinematic boundary conditions are applied on the structure, the seabed and the free surface. It states that there can be no flow through the surface of the structure or the seabed (Equation 2.4), and that the fluid particles on the free surface do not leave the free surface (Equation 2.5).

$$\left.\frac{\partial\phi}{\partial n}\right|_{surface} = 0 \tag{2.4}$$

$$\frac{\partial\zeta}{\partial t} = \frac{\partial\Phi}{\partial z} \tag{2.5}$$

In addition the dynamic boundary condition (Equation 2.6) must be held. Which states that the pressure on the surface must be equal to the atmospheric pressure. Note that the kinematic free surface condition (2.5) and dynamic free surface condition (2.6) are derived from non-linear relations situated at the free surface. Since the free surface is unknown, the terms are linearised to apply for the mean free surface. Then it is applied for linear theory, so that Equation 2.5 and 2.6 hold for $z = 0$, oppose to for $z = \zeta$, which is the non-

linear term.

$$g\zeta + \frac{\partial \Phi}{\partial t} = 0 \tag{2.6}$$

These equations are collected from Faltinsen [1993], where the velocity potential for the incident wave in deep water depths is derived from the boundary value problem. The result is Equation 2.7, for regular waves propagating in the x-direction[1] .

$$\phi(x, y, z, t) = \frac{g\zeta_a}{\omega} e^{kz} cos(\omega t - kx) \tag{2.7}$$

Where $k = \frac{\omega^2}{g}$, known as the dispersion relation and $z = 0$ at the mean surface, and positive in upwards vertical direction.

2.1.2 Obtaining the Dynamic Equation of Motion

Since the problem is now linear it is possible to split the velocity potential into terms dependent on diffraction and radiation. When solving the linear wave-induced problem it is convenient to separate the loads connected to excitation, by considering a fixed structure subjected to incoming waves. Then consider the surface to be undisturbed while moving the structure in six degrees of freedom, to obtain the added mass, damping and restoring forces. By superposition the solution for the complete response of the structure subjected to waves are found.

The solution of the radiation and diffraction velocity potentials is obtained by a panel method. This is a numerical method to solve for wave-induced motions and loads. The wet surface of the structure is discretized into panels, where the source strengths are assumed to be constant over each panel. The velocity potentials are then computed from the solution of an integral equation, obtained by using Green's Theorem (DNV [2010]).

[1] Note that Wadam applies a different expression for the velocity potential. Which accounts for both finite and infinite water depths.

The equation system is very complex and indefinite, and can be solved in Wadam by an iterative method or direct LU-factorisation method.

In Equation 2.8, the Morison equation that is applied in Wadam is presented (from DNV [2010]), where **B** is the viscous damping matrix that has to be linearised for application in FD.

$$\mathbf{F}(\omega) = \omega^2(\mathbf{M} + \rho V_M \mathbf{C_a})\xi - \omega^2 \rho V_M(\mathbf{C_a} + \mathbf{I})\mathbf{x} + i\omega\mathbf{B}(\mathbf{x} - \xi) + \mathbf{f}_c + \mathbf{f}_g + \mathbf{f}_b \tag{2.8}$$

Where, V_M is the displaced volume of the Morison element, ξ and **x** are the complex amplitude of the motion and incident wave respectively. Then **f**, are fluctuating forces from restoring, gravity or buoyancy dependent on subscript c, g and b respectively. And C_a contains the added mass coefficients.

The drag force (Equation 2.9) is proportional to the relative motion between the incident wave and structure squared, hence it must be linearised for application in FD-method. This can be approximated by rewriting the equation with a linearisation coefficient, B_L^*. By introducing the relative velocity as harmonic terms, the error is minimized by assuming equal work for the two terms by integrating the error squared over one period. The minimum error will then be obtained by solving for the partial derivative of the error, with respect to the linearised coefficient as seen in Equation 2.10.

$$\mathbf{F}_D = \frac{1}{2}\rho\sigma\mathbf{C}_D(\mathbf{v} - \dot{\mathbf{x}})|\mathbf{v} - \dot{\mathbf{x}}| \approx \frac{1}{2}\rho\sigma\mathbf{C}_D B_L^*(\mathbf{v} - \dot{\mathbf{x}}) \tag{2.9}$$

Where σ is the projected area of the Morison element, $\mathbf{C}_D$ contains the drag coefficients, and $\mathbf{v} - \dot{\mathbf{x}}$ is the relative velocity between the incident wave and the structure.

$$\frac{\partial \bar{e}^2}{\partial B_L^*} = 0 \tag{2.10}$$

General solution for this is presented in Equation 2.11.

$$B_L^* = \frac{8}{3\pi} V_{max} \tag{2.11}$$

From the solution of the panel model and Morison model the added mass, damping and exciting force contributions in Equation 2.1 are obtained. Then it is possible to solve for the motions in six degree of freedom by assuming that the motions and the force can be described as in Equation 2.12. The dynamic equation of motion can be simplified to Equation 2.13.

$$\begin{aligned}\mathbf{Y}(\omega) &= \mathbf{Y}_0 e^{i\omega t} \\ \dot{\mathbf{Y}}(\omega) &= i\omega \mathbf{Y}_0 e^{i\omega t} \\ \ddot{\mathbf{Y}}(\omega) &= -\omega^2 \mathbf{Y}_0 e^{i\omega t} \\ \mathbf{F}(\omega) &= \mathbf{F}_0 e^{i\omega t}\end{aligned} \tag{2.12}$$

$$\Big[-\omega^2(\mathbf{M}+\mathbf{A}(\omega)) + i\omega\mathbf{B}(\omega) + \mathbf{C} \Big] \mathbf{Y}_0 e^{i\omega t} = \mathbf{F}_0 e^{i\omega t} \tag{2.13}$$

From Equation 2.13, the force to motion transfer function is obtained as Equation 2.14, giving the relation between external force and motion for six degree of freedom (dof).

$$\mathbf{H}_{FY}(\omega) = \Big[-\omega^2(\mathbf{M}+\mathbf{A}(\omega)) + i\omega\mathbf{B}(\omega) + \mathbf{C} \Big]^{-1} \tag{2.14}$$

2.1.3 From Time-Domain to Frequency-Domain

In order for the frequency domain method minimize error compared to time-domain solutions, it is necessary to implement as much as possible of the second order loads into the linear solution of the equation of motion. The second order loads are based on the second order potential, which is non-linear. It is however possible to extract some of the 2nd order effects from the 1st order potential, and these contributions to the full solution will be implemented. The contributions which are possible to implement in a frequency domain method, by application in Wadam, are the mean drift loads and the slowly varying drift forces. This can be described in the frequency domain by quadratic transfer functions. Following is a description on how to go from time-domain to frequency do-

main, by application of Fourier transformation. The external force is now split into two terms, one describing the linear wave induced force, and one describing the second order force. Eventually force and motion spectrum are obtained, which can be applied in FD-analysis.

In order to apply the equations for the hydrodynamic loads that are presented in this section it is necessary to make some assumptions about the surface elevation. The stochastic process is assumed to be stationary, which yields that it is independent on time instants, and is only dependent on the length of the time interval. The prosess is also assumed to be ergodic, which means that the process' statistical properties can be deducted from one random sample. Which implies that they can be determined by time-averaging rather than ensemble averaging. The process is described by a Gaussian (normal) distribution with a mean value of zero. The equations for deriving the spectral density for second order forces that are presented here were acquired in Moan [2009], and a similar approach can be found in Section 11.3 in Naess and Moan [2013]. For more basic information on the theory the reader is revised to look up chapter 3-6 in Newland [1993].

For the rest of this section the subscript denotes whether it is second order contribution or first order contribution, by 2 or 1 respectively in the functions (as in Equation 2.15). While for frequency or time variables 1 and 2 only describes that there are two different values.

The linear hydrodynamic loads are proportional to the wave elevation, while the non-linear forces that are described here, only contains contributions for the 2nd order loads that are proportional to the wave elevation squared. Similar derivations could be done for higher order loads, but these are not investigated here. The total force can then be described as a sum of the first order and the second order loads as shown in Equation 2.15.

$$f(t) = f_1(t) + f_2(t) \tag{2.15}$$

Where the linear force can be represented by a linear impulse response function propor-

tional to the surface elevation, as Equation 2.16. The second order contribution can be described by a quadratic impulse response function proportional to the surface elevation squared, as in Equation 2.17.

$$f_1(t) = \int_{-\infty}^{\infty} h_1(t_1)\zeta(t-t_1)dt_1 \tag{2.16}$$

$$f_2(t) = \int_{-\infty}^{\infty}\int_{-\infty}^{\infty} h_2(t_1,t_2)\zeta(t-t_1)\zeta(t-t_2)dt_1dt_2 \tag{2.17}$$

The expressions for the linear and second order forces are now time-dependent, while it is of interest to present it as frequency dependent terms. This can be done by applying direct Fourier transformation, as described by Equation 2.18.

$$\mathscr{F}\big[f(t)\big] = F(\omega) = \int_{-\infty}^{\infty} f(t)e^{-i\omega t}dt \tag{2.18}$$

The surface elevation, $\zeta(t)$, can be expressed as a frequency-dependent term by Fourier transform, as in Equation 2.18 [2]. In the lecture notes from Moan [2009], 2.19 and 2.20 are used for direct and indirect Fourier transformation respectively.

$$Z(\omega) = \mathscr{F}\big[\zeta(t)\big] = \int_{-\infty}^{\infty} \zeta(t)e^{-i\omega t}dt \tag{2.19}$$

$$\zeta(t) = \mathscr{F}^{-1}\big[Z(\omega)\big] = \frac{1}{2\pi}\int_{-\infty}^{\infty} Z(\omega)e^{i\omega t}d\omega \tag{2.20}$$

When establishing a frequency domain method it is adequate to express the link between the surface elevation and forces by use of transfer functions. A linear transfer function can be obtained by Fourier transformation of the impulse response function as shown in Equation 2.21. While the quadratic transfer function (QTF) are dependent on two frequencies, obtained by double Fourier transform over two time-variables (Equation 2.22). The diagonal of the QTF yields that $\omega_i = \omega_j$, hence these are linked to the mean drift forces,

[2] Note that there exists different expressions of the definition of Fourier and inverse Fourier transform, where the constant prior to the integration is different, these solutions are however equivalent representations.

while the off-diagonal terms are linked to the slowly varying forces.

$$H_1(\omega) = \int_{-\infty}^{\infty} h_1(t) e^{-i\omega t} dt \tag{2.21}$$

$$H_2(\omega_1, \omega_2) = \int_{-\infty}^{\infty}\int_{-\infty}^{\infty} h_2(t_1, t_2) e^{-i(\omega_1 t_1 + \omega_2 t_2)} dt_1 dt_2 \tag{2.22}$$

Two of the symmetry relations of the transfer functions are presented in Equation 2.23 and 2.24[3].

$$H_1(\omega) = H_1^*(-\omega) \tag{2.23}$$

$$H_2(\omega_1, \omega_2) = H_2^*(-\omega_1, -\omega_2) \tag{2.24}$$

By use of the above equations, the linear and second order force, Equation 2.16 and 2.17, can now be rewritten by Fourier and double Fourier transformation into Equation 2.25 and 2.26.

$$f_1(t) = \frac{1}{2\pi}\int_{-\infty}^{\infty} H_1(\omega) Z(\omega) e^{i\omega t} d\omega \tag{2.25}$$

$$f_2(t) = \frac{1}{4\pi^2}\int_{-\infty}^{\infty}\int_{-\infty}^{\infty} H_2(\omega_1, \omega_2) Z(\omega_1) Z(\omega_2) e^{i(\omega_1+\omega_2)t} d\omega_1 d\omega_2 \tag{2.26}$$

It is however not of interest to have the forces as a function of time, but as a function of frequency, and the following relations must apply (Equation 2.27 and 2.28). Since it is adequate to present the second order force as a function of one input, substitution is performed by $\omega = \omega_1 + \omega_2$ for the second order force.

$$F_1(\omega) = H_1(\omega) Z(\omega) \tag{2.27}$$

$$F_2(\omega) = \frac{1}{4\pi^2}\int_{-\infty}^{\infty} H_2(\omega_1, \omega - \omega_1) Z(\omega_1) Z(\omega - \omega_1) d\omega_1 \tag{2.28}$$

[3]Superscript * represent complex conjugate.

For the rest of this section a procedure to obtain the second order spectral density (from Moan [2009]) is explained. For more information on the relationship and properties of the autocorrelation function and spectral density, see Moan [2009] and Chapter 3-6 in Newland [1993]. The aim is to establish an expression for the spectral density of the second order force, and due to these relations the procedure starts with the autocorrelation function.

The autocorrelation function of the second order force, is in general described as in Equation 2.29, where E means the expected value of the stochastic process. It is of interest to rewrite this equation in terms of frequency dependent functions.

$$R_{f_2 f_2}(\tau) = \mathrm{E}[F_2(t-\tau)F_2(t)] - (\mathrm{E}[F_2(t)])^2 \tag{2.29}$$

By introducing the autocorrelation function for the wave elevation, the following relation between the autocorrelation function and the wave spectrum applies (2.30).

$$R_{\zeta\zeta}(\tau) = \frac{1}{2\pi}\int_{\omega} S_{\zeta\zeta}(\omega)e^{i\omega\tau}d\omega \tag{2.30}$$

By inserting Equation 2.30 into 2.29 the autocorrelation function for the second order force is now dependent on the quadratic transfer function and the wave spectrum (Equation 2.31).

$$R_{f_2 f_2}(\tau) = 2\int_{\omega_1}\int_{\omega_2} H_2(\omega_1,\omega_2)H_2(-\omega_1,-\omega_2)S_{\zeta\zeta}(\omega_1)S_{\zeta\zeta}(\omega_2)e^{i(\omega_1+\omega_2)\tau}d\omega_1 d\omega_2 \tag{2.31}$$

To simplify the expression, substitute $\mu = \omega_2$ and $\omega = \omega_1 - \omega_2$ into Equation 2.31, to acquire the second order forces due to difference frequency (if sum-frequency forces are of interest apply $\omega = \omega_1 + \omega_2$). In addition, apply the symmetry properties for the quadratic transfer functions as given in Equation 2.24. The result is then Equation 2.32, which can, due to the substitution solely be dependent on ω. Which is preferable in order to use superposition

later.

$$R_{f_2 f_2}(\tau) = 2\int_{\omega}\int_{\mu} H_2(\omega+\mu,\mu)H_2^*(\omega+\mu,\mu)S_{\zeta\zeta}(\omega+\mu)S_{\zeta\zeta}(\mu)e^{i\omega\tau}d\omega d\mu \tag{2.32}$$

By applying the relation between spectral density and autocorrelation function 2.33.

$$S_{F_2F_2}(\omega) = \int_{\tau} R_{f_2 f_2}(\tau)e^{i\omega\tau}d\tau \tag{2.33}$$

The final formula for the 2nd order spectral density becomes :

$$S_{F_2F_2}(\omega) = 2\int_{\mu} H_2(\omega+\mu,\mu)H_2^*(\omega+\mu,\mu)S_{\zeta\zeta}(\omega+\mu)S_{\zeta\zeta}(\mu)d\mu \tag{2.34}$$

The motion spectrum for the structure can then be obtained by Equation 2.35, where both the linear and difference frequency force are accounted for. Where i denotes which degree of freedom that is investigated, and H_{FY_i} is the corresponding row in the force to motion transfer function in Equation 2.14.

$$S_{Y_iY_i}(\omega) = |H_{\zeta Y_i}(\omega)|^2 S_{\zeta\zeta}(\omega) + |H_{FY_i}(\omega)|^2 S_{F_2F_2}(\omega) \tag{2.35}$$

Timeseries can then be easily be obtained by Equation 2.36, where θ_k is a random phase angle.

$$Y_i(t) = \sum_{k=1}^{N}\sqrt{2S_{Y_iY_i}(\omega_k)\Delta\omega}cos(\omega_k t+\theta_k) \tag{2.36}$$

2.2 Establishing a FD-Method for Aerodynamic Loads

This section gives an introduction to the boundary value problem from ideal momentum theory, over to presenting basic aerodynamic foil theory and how this is applied in two methods for calculating the aerodynamic loading on a rotor; Blade/element Momentum (BEM) and Generalized Dynamic Wake (GDW). In addition, an introduction to how some of the dynamic problems on a wind turbine are solved in TD-simulations and FD-methods.

Following, a short note on wind properties in Section 2.3. And finally, the state-space model applied in order to obtain the external forces from wind are presented in 2.2.2.

2.2.1 Basic Aerodynamic Theory

Since the study programme marine technology has had little focus on aerodynamic theory, some of the basics will be presented here in order for the reader to comprehend more of the state-space model presented in Section 2.2.2. Derivation of the ideal momentum theory will not be elaborated here, but can be found in Hansen [2008] or Bachynski [2015a]. The boundary value problem for ideal momentum theory is governed by conservation of mass and conservation of momentum in the control volume surrounding the rotor disk. The applied assumptions (from Hansen [2008]) are;

1. Homogeneous, incompressible and steady state flow.
2. No frictional drag.
3. Infinite number of blades and uniform thrust over the rotor-disk.
4. Irrotational flow.
5. Continuous velocity over the rotor disk.
6. pressure equal to atmospheric pressure far from the disk

Some of these assumptions are removed for practical applications. Following is a brief introduction to foil theory , and two approaches to calculate the aerodynamic loads;
blade/element momentum (BEM) and generalized dynamic wake (GDW), all of which originates from ideal momentum theory.

Foil Theory

To understand how the rotor extracts energy from the wind it is important to know some basics on foil theory. A foil is the cross-section of a rotor blade, which varies from the centre of the rotor to the tip. This is carefully designed to generate lift. The foil has a larger distance for the wind to pass on one side than the other side. All of the air does however

have to pass, therefore the velocity of the particles that has to travel a longer distance is increased, relative to the particles that travel a shorter distance, causing lower pressure on the top side, relative to the other side. This causes a suction, or a lift force, making the blade rotate about the shaft.

The direction of the lift force is perpendicular to the angle of attack, which defines the angle between the chord line and the angle of the relative velocity applied on the turbine. The relative velocity is dependent on the incoming velocity, the rotation of the turbine and the induced axial and tangential velocity at the blade. The drag force on the cross-section of the blade is parallel to the relative velocity. The lift and drag forces are dependent on Reynolds number:

$$Rn = \frac{UD}{\nu} \tag{2.37}$$

Where U is the incoming velocity, D is the significant length, and ν is the kinematic viscosity. According to the Magnus effect, the rotating blades cause rotation in the flow. In foil theory the rotation is expressed by circulation. Dependent on the Reynolds number, a relation between the lift coefficient and the angle of attack can be deduced. Here important properties of the lift can be observed. For low angle of attack the flow is attached and the lift force has a linear increase. Then it begins to stall, the foil lose lift and in the fully stalled regime there is almost just drag-forces, which yields that the turbine has stopped. This can be described by Figure 2.1, where you see the relation between lift, drag and pitching moment dependent on the angle of attack. These are the characteristics of one foil in the 5MW NREL turbine (Jonkman et al. [2009]), and the curves would alter dependent on geometry and Reynolds number.

Dynamic Stall

Dynamic stall is caused by oscillatory or unsteady angle of attack. The angle of attack is dynamic due to horizontal and vertical shear in the wind, vertical wind, yaw misalignment and turbulence. The overall consequence is that there is a variation in the velocity over

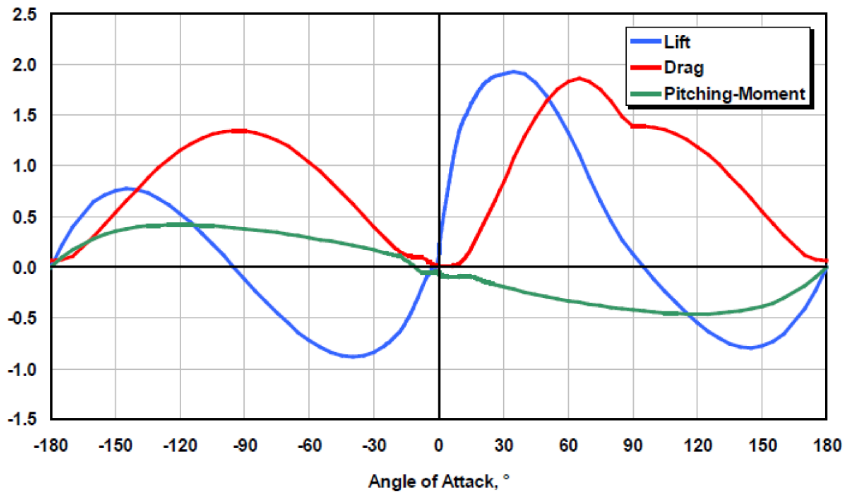

Figure 2.1: Relation between lift, drag and pitch coefficients for different angle of attack, for a DU40 airfoil (in courtesy of Jonkman et al. [2009]).

the rotor. As mentioned before, the angle of attack is parallel to the drag force and normal to the lift force, hence dynamic stall cause change in the contribution from lift and drag coefficients. This is a complex problem, and one of the corrections that can be made is applying Beddoes-Leishman method. This method is semi-empirical, and modifies the response based on the effective flow separation point on the suction side of the airfoil. In addition the time-lag between change in angle of attack and actual change in aerodynamic behaviour must be considered (Moriarty and Hansen [2005]). Working in the frequency domain a linear relationship must be used, an implementation of the Øye model that Merz et al. [2012] has used is preferable to the alternative of using the quasi-static lift coefficients in Figure 2.1, as described in Section 1.2.4.

Blade/Element Momentum Theory

The blade/element momentum (BEM) originates from foil theory and the ideal momentum theory. The key difference will be discussed here. First of all, the BEM-method considers the normal force on the airfoil, so it alters contribution from drag and lift forces to be applied in normal and tangential direction of the airfoil. The procedure of BEM require iteration over the axial induction factor and the angular induction factor. In addition, the assumption of infinite number of blades must be corrected for and consequently the axial

induction factor is altered.

Prandtl's correction:

To account for that there is a finite number of blades Prandtl has developed a correction factor. The reason is that with a finite number of blades the wake downstream of the turbine is quite different than when assuming an infinite number of blades. Figure 2.2 shows how the vortices from one blade are moving downstream of a rotating turbine. Prandtl tried to capture this effect by describing the wake as vortex sheets that follows the mean flow velocity and has no direct influence on the wake itself. It is important to account for this tip-loss effect, because the thrust force at the tip is reduced compared to when it is not included.

Glauert's correction:

There is a problem with the axial induction factor as it exceeds 0.5. This indicates that the turbine is operating with a high tip speed ratio, which yields that the incoming wind velocity is small compared to the rotational frequency of the rotor. If it is not corrected, it implies that the velocity in the far wake is negative, hence moving back to the turbine. This is not physical and must be corrected for. The physical solution is that more flow that is not initially participating in the wake, enters the wake stream, which cause more turbulence. The flow behind the rotor will decrease, but not become negative, consequently the thrust on the rotor increase. Solution to this problem is applying Glauert's correction for axial induction factor greater than 0.4. A relation between the thrust and axial induction factor is established based on empirical data from experiments on a helicopter with high induced velocities. As in the derivation of the ideal momentum theory it was initially used for correcting the pressure difference across the rotor disk for the 1D problem, however now it is developed to also account for local coefficients at the elements of the blades. This implies that it is considered together with Prandtl's tip-loss factor.

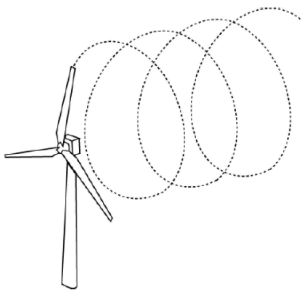

Figure 2.2: The wake from the tip of one blade on a rotating turbine (in courtesy of Moriarty and Hansen [2005]).

Generalized Dynamic Wake Theory

For lightly loaded rotors, Generalized Dynamic Wake (GDW) is the preferred theory to apply for calculating the loads on the wind turbine. For the 5MW NREL turbine GDW should be applied for incoming wind velocity greater than approximately 8 m/s in SRA. GDW is not an iterative process, and is suited for dynamic inflow, yawed inflow and for higher wind speed. It covers the dynamic wake effect by calculating the aerodynamic loading on the rotor blades by a Laplace formulation. The Laplace equation consists of a description on the velocity potential, where the velocity potential is divided into one space varying component and one time-varying component. The method originates from Euler Equations for conservation of momentum and conservation of mass. The assumptions required for GDW are: assumption 6, from before, that pressure is equal to atmospheric pressure far from the disk. In addition, that the forces on the rotor are aerodynamic loading, inviscid flow and finally that the pressure loss over the disk is equal to the thrust force from the rotor. The method has a potential flow solution to the Laplace Equation, where the Laplace Equation consists of 1st order differential equations: Legendre functions and trigonometric functions. The GDW method takes into account the phenomena of dynamic wake. Dynamic wake can be described as a time-lag of the induced velocities caused by vortex shedding. A physical interpretation of this is that the power has a dynamic behaviour responding to for example a rapid change in blade pitch, so that it will get a transient amplitude due to these changes before it stabilizes at a point close to the solution provided by BEM (where dynamic wake is not accounted for). The mathematics of this procedure is ex-

tensive, the derivation of this method can be found in Moriarty and Hansen [2005].

2.2.2 Linear State-Space Analysis

Merz [2015b] has established a state-space (STAS) method for calculating the linear dynamic equation of motion on an offshore wind turbine. The basis for a STAS method is described by equations written in the form of Equation 2.38 and 2.39.

$$\frac{d\mathbf{x}}{dt} = \mathbf{A}\mathbf{x} + \mathbf{B}\mathbf{u} \tag{2.38}$$

$$\mathbf{y} = \mathbf{C}\mathbf{x} + \mathbf{D}\mathbf{u} \tag{2.39}$$

For application in this thesis the states, inputs and outputs of these equations include;

- **x** contains the system of states; tower, nacelle, driveshaft and rotor elastic modes, in addition to their time derivatives.
- **u** the input, the turbulent wind speed in rotor coordinates.
- **y** the output, aerodynamic forces in rotor coordinates.

For this purpose, it is more convenient to write Equation 2.38 with a sparse matrix, but 2.38 and 2.40 are equivalent.

$$\mathbf{L}\frac{d\mathbf{x}}{dt} = \mathbf{A}\mathbf{x} + \mathbf{B}\mathbf{u} \tag{2.40}$$

It is more appropriate to describe the state-space model as a collection of linked modules. Then, local descriptions in state-space form can be linked into a global solution as in Equation 2.41 and 2.42.

$$\mathbf{L}\frac{d\mathbf{x}}{dt} = \widetilde{\mathbf{A}}\mathbf{x} + \mathbf{B_u}\mathbf{u} + \mathbf{B_y}\mathbf{y} \tag{2.41}$$

$$\mathbf{y} = \widetilde{\mathbf{C}}\mathbf{x} + \mathbf{D_u}\mathbf{u} + \mathbf{D_y}\mathbf{y} \tag{2.42}$$

The **y** on the right hand side is still the global output as in Equation 2.39, but the **y**-matrices associated with $\mathbf{B}_y$ and $\mathbf{D}_y$ are treated as a local input in the current state, but is actually representing a local output from a different module. In order to eliminate **y** from the right-hand side, the expressions were manipulated in Merz [2015b] into Equation 2.43 and

2.44.

$$\mathbf{L}\frac{d\mathbf{x}}{dt} = \left[\widetilde{\mathbf{A}} + \mathbf{B_y}\left(\mathbf{I} - \mathbf{D_y}\right)^{-1}\mathbf{D_u}\right]\mathbf{x} + \left[\mathbf{B_u} + \mathbf{B_y}\left(\mathbf{I} - \mathbf{D_y}\right)^{-1}\mathbf{D_u}\right]\mathbf{u} \tag{2.43}$$

$$\mathbf{y} = \left(\mathbf{I} - \mathbf{D_y}\right)^{-1}\widetilde{\mathbf{C}}\mathbf{x} + \left(\mathbf{I} - \mathbf{D_y}\right)^{-1}\mathbf{D_u}\mathbf{u} \tag{2.44}$$

A detailed procedure on how to obtain the dynamic problem in state-space form is described in Merz [2015b], the outline will be presented here. The procedure is as follows;

1. Discretize the system into modules depending on different operations of physical processes.
2. Establish the governing equation for each module.
3. Linearise the module so that 2nd order terms are not introduced in 2. by use of perturbation theory, so that only the 1st order terms remains.
4. Separate between global and local inputs, and express them in a linear state-space form as in Equation 2.40 and 2.39.

Aerodynamic Loads on the Rotor

For calculation of the aerodynamic loads Blade/element Momentum (BEM) is used. This is implemented to include Prandtl's tip loss function, dynamic inflow, circulation lag and dynamic stall. Dynamic inflow and dynamic stall are accounted for by Øye-model as described in Section 1.2.4. As explained in Section 2.2.1, BEM is an interative procedure and the aerodynamic loads are obtained as follows :

1. Induced velocities are calculated by momentum balance on the airfoils of the discretized structure.
2. Dynamic inflow is estimated by the Øye-model.
3. 1. and 2. are used to estimate the instantaneous angle of attack.
4. From 3. the change in lift on the airfoil is obtained and modelled as a time lag for the angle of attack and dynamic stall.
5. 4. gives modified lift and drag coefficients.
6. 5. is used to calculate the corresponding forces, in addition to the local velocity at the blade.

7. 6. is transformed from section coordinates into rotor coordinates to return to 1. for momentum balance.
8. If the momentum balance is satisfied, 6. is transformed into blade pitch coordinates for calculating structural modes.

Structural Model in STAS

The structural model is constructed by finite element (FE) beam description, assuming small displacements. Standard beam theory is used to obtain the FE mass, stiffness and damping matrices, only careful considerations to be made for implementing structural damping by a modal approach (calculating the damping from eigenvalue problem of the state-space formulation). In addition, in order to obtain correct natural frequencies of the structure, centrifugal stiffening is included. Centrifugal stiffening is present due to the deflection of the blades about a mean point. The dynamic equation of motion is a simplified multibody formulation. Lagrange Equations are used for this purpose, acquired by investigating an energy dissipation formulation. Nodal forces in the FE-beams are obtained by principle of virtual work (PVW). The linear solution to be used in FD-analysis is obtained by evaluating the formulations in steady-state. In Merz [2015b] derivations of the expressions for potential and kinetic energy, PVW and equation of motion are presented, but the formulas are extensive so they will not be included here. The resulting equation of motion in state space form is Equation 2.45, where $\mathbf{q_1} = \mathbf{q}$ and $\mathbf{q_2} = \frac{d\mathbf{q}}{dt}$ as in Equation 2.40 and 2.39[4].

$$\begin{bmatrix} \mathbf{I} & \mathbf{0} \\ \mathbf{0} & \mathbf{M} \end{bmatrix} \frac{d}{dt} \begin{bmatrix} \mathbf{q_1} \\ \mathbf{q_2} \end{bmatrix} = \begin{bmatrix} \mathbf{0} & \mathbf{I} \\ -\mathbf{K} & -\mathbf{C} \end{bmatrix} \begin{bmatrix} \mathbf{q_1} \\ \mathbf{q_2} \end{bmatrix} + \begin{bmatrix} \mathbf{0} \\ \Delta\mathbf{F} \end{bmatrix} \tag{2.45}$$

[4] In conjunction to the dynamic equation of motion (Equation 2.1), **K** would represent the stiffness term, **C** would represent the damping term.

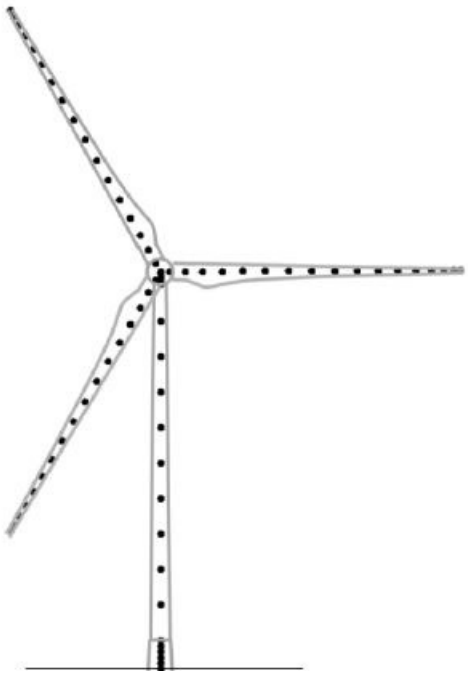

Figure 2.3: Example on how the WT is discretized into beam elements (in courtesy of Merz [2015b]).

Transfer Functions

By assuming harmonic motion, the state, input and output matrices can be written as in Equation 2.46. Then it is possible to write the state-space form, Equation 2.40 and 2.39, as Equation 2.47 and 2.49 respectively.

$$\begin{aligned} \mathbf{u} &= \mathbf{u}_0 e^{i\omega t} \\ \mathbf{y} &= \mathbf{y}_0 e^{i\omega t} \\ \mathbf{x} &= \mathbf{x}_0 e^{i\omega t} \\ \frac{d\mathbf{x}}{dt} &= i\omega \mathbf{x}_0 e^{i\omega t} \end{aligned} \tag{2.46}$$

$$(i\omega \mathbf{L} - \mathbf{A})\mathbf{x}_0 = \mathbf{B}\mathbf{u}_0 \tag{2.47}$$

From Equation 2.47 the transfer function between the states and input can be obtained as Equation 2.48. This can again be inserted for $\mathbf{x}_0$ in Equation 2.39 to write output as a

function of input as in Equation 2.49.

$$\mathbf{H}_{ux}(\omega) = (i\omega\mathbf{L} - \mathbf{A})^{-1}\mathbf{B} \tag{2.48}$$

$$\mathbf{y}_0 = \big(\mathbf{C}\mathbf{H}_{ux}(\omega) + \mathbf{D}\big)\mathbf{u}_0 \tag{2.49}$$

From Equation 2.49, the transfer function between output and input is obtained as Equation 2.50.

$$\mathbf{H}_{uy}(\omega) = \mathbf{C}\mathbf{H}_{ux}(\omega) + \mathbf{D} \tag{2.50}$$

Integrating the Aerodynamic Force

The aerodynamic forces that are output from the state-space model are given in rotor coordinates/MBC, distributed over the blade elements of the rotor. The blades are modelled with 16 elements each. In order to properly transform the external force from the rotor to the global coordinate system, the aerodynamic loads must be integrated over the rotor. This gives an resulting thrust force at the hub, and a torque moment over the shaft, which are the most significant loads on the rotor. Thus, the remaining forces on the rotor are neglected. When integrating the forces over the rotor, the tilt angle of the rotor is assumed to be negligible. So that the forces on the rotor are parallel to the global coordinate system.

The aerodynamic loads obtained from the state-space model are in the rotor coordinate system. This type of coordinate-system is usually referred to as multi-blade coordinates (MBC), which are used for the process in order to represent the dynamics of the turbine properly. MBC has a collective axial and in-plane component, and sine- and cosine- components of the axial and in-plane forces. The axial component is parallel to the rotor Z-axis, which passes through the hub to the tower. We assume that there is no tilt angle on the nacelle, and therefore the rotor Z-axis is parallel to the global X-axis, with a vertical distance of the hub-height in between. With no tilt on the rotor-cone the rotor Y-axis is parallel to the global Z-axis, and the rotor x-axis is parallel to the global y-axis. A description of the difference between the global and the rotor coordinate system is given in Figure

2.4.

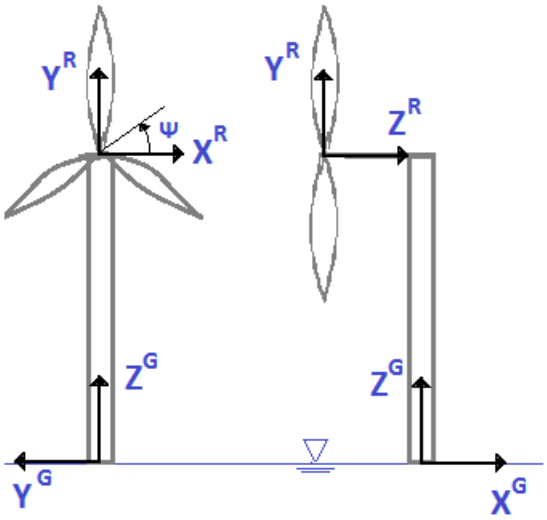

Figure 2.4: Superscript R and G, for rotor-coordinates and global coordinates respectively. Ψ denotes the Azimuth angle.

The resulting thrust force and torque are then transformed to global coordinates under the assumptions above. This will give a pitching moment from the thrust force by the transformation in Equation 2.51, a force in x-direction directly related to thrust as in Equation 2.52 and a roll moment due to the torque at the rotor as in Equation 2.53.

$$M_Y^G = F_z^R \Delta z^G \tag{2.51}$$

Where Δz^G is the vertical distance between the mean waterline and the hub.

$$F_X^G = F_z^R \tag{2.52}$$

$$M_X^G = M_Z^R \tag{2.53}$$

Spectrum

H_{uy}, was from previous a matrix. But for this application, the terms are summarized into a column matrix, with the size of the number of elements over the blades in collective axial

MBC. Consequently the size of H_{uy} is then a 16x1 vector. The wind spectrum is a 16x16 matrix, including the corresponding cross-spectra for the blade elements. Then the thrust force spectra can be acquired by Equation 2.54, for one frequency.

$$S_{yy}(\omega_i) = \mathbf{H}_{uy}^T(\omega_i)\mathbf{S}_{uu}(\omega_i)\mathbf{H}_{uy}^*(\omega_i) \tag{2.54}$$

Transformation to global coordinates then yields that the force from wind in x-direction can be written as Equation 2.55, and the corresponding pitching moment can be written as Equation 2.56[5].

$$S_{F_1^u F_1^u}(\omega) = S_{yy}(\omega) \tag{2.55}$$

$$S_{F_5^u F_5^u}(\omega) = S_{yy}(\omega)(\Delta z^G)^2 \tag{2.56}$$

2.3 Properties of Wind

Different properties can be prescribed to the wind field, the most important ones will be mentioned here. Turbulent wind varies in both velocity and direction, the wind field can be generated based on different wind-spectra, e.g. the Kaimal spectrum:

$$S_K(f) = \frac{4\sigma_K^2 L_K/\bar{U}_{hub}}{(1+6fL_K/\bar{U}_{hub})^{\frac{5}{3}}} \tag{2.57}$$

Where K denotes three directions for the wind, σ_K is the standard deviation of the wind in the different directions, $\bar{U}_{hub}$ is the mean wind speed at hub height, f is the circular frequency and L_K is an integral scale parameter which is dependent on the turbulence.

From Figure 2.5, a representation of a turbulent wind field for application in SRA can be seen. The grid-spacing is the distance between each of the squares, and should not be

[5]Note the distinction between uppercase and lowercase, y is related to the output in the state-space model, while Y is related to the global motions.

larger than the chord length of the blades on the wind turbine. The properties of the grid is length, breadth and number of points where a velocity, and its directions are defined. The grid has to be larger than the diameter of the rotor. The larger the turbulence intensity is defined as, the larger the variations of the wind speed will be.

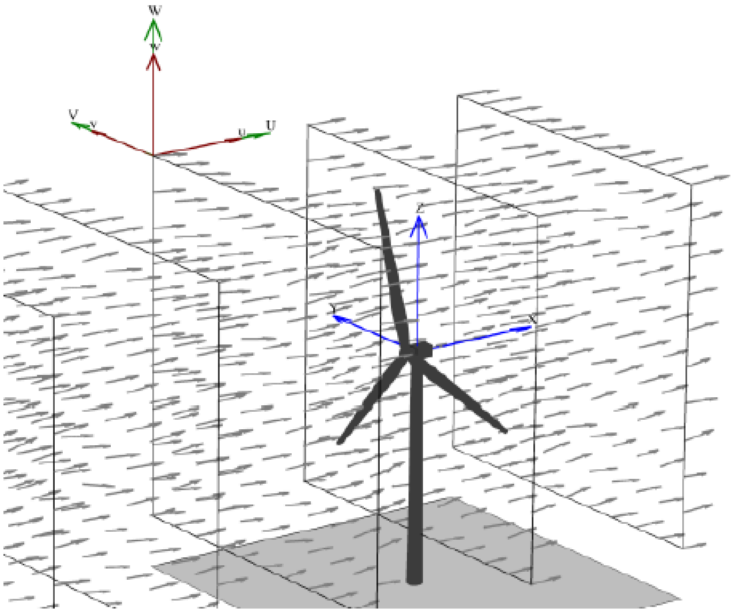

Figure 2.5: Turbulent wind field (in courtesy of Jonkman [2009])

An illustration of wind with a shear profile is shown in Figure 2.6. As you can see from the figure the velocity is increasing with the height, which in general will give a higher wind speed at the top of the rotor than it is at the lower part.

For application in frequency domain, the wind must be represented in a different manner. Merz [2015a] has established a description of the atmospheric turbulence by starting with a single-point von Karman spectrum:

$$S_{zz}^{0} = \sigma_u^2 \frac{4L_u}{V_\infty [1 + 70.8(fL_u/V_\infty)^2]^{\frac{5}{6}}} \tag{2.58}$$

Correlation in time can then be represented by an inverse Fourier transform of 2.58 as shown in Equation 2.59. Again correlated to space, by replacing 0 with a space variable. For this purpose, the space variable is used to describe position on the blade.

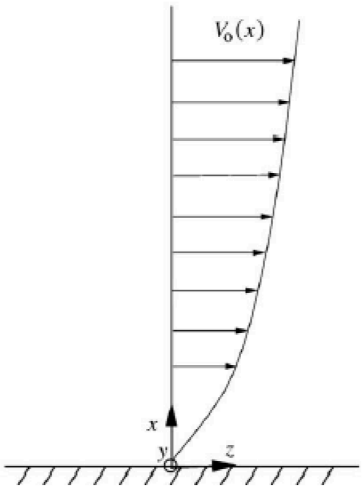

Figure 2.6: Wind shear profile (in courtesy of Hansen [2008]).

$$Q_{zz}(0,\tau) = \frac{2\sigma_u^2}{\Gamma(1/3)}\left(\frac{V_\infty \tau}{2.68L_u}\right)K_{1/3}\left(\frac{V_\infty \tau}{1.34L_u}\right) \tag{2.59}$$

The wind spectrum can then be obtained by Fourier transform of the correlation function, as given in Equation 2.60. However, for application in a state-space model it is most convenient to represent the spectrum in multi-blade coordinates (MBC). The collective component, representing the wind parallel to the z-axis in rotor coordinates, can be written as in Equation 2.61.

$$S(f) = \int_{-\infty}^{\infty} Q(\tau) exp(-i2\pi f\tau) d\tau \tag{2.60}$$

$$Q_{00}^{\psi}(r_1, r_2, \tau) = E\left[u_0^{\psi}(r_1, t) u_0^{\psi}(r_2, t+\tau)\right] \tag{2.61}$$

Where the relation to the blade coordinates are as in Equation 2.62, where subscript 1,2,3, yields blade number. On the contrary to the wind-field applied in SRA, as graphically presented in Figure 2.5, the wind input in a state-space model is described as cross-spectra for specified points on the rotor blades in the frequency domain. An example is presented in Figure 2.7, where S_{zz} is the collective axial component, and S_{tt} is the collective in-plane component.

$$Q_{00}^{\psi}(r_1, r_2, \tau) = \mathrm{E}\Big[\frac{1}{3}(u_1(r_1,t) + u_3(r_1,t) + u_1(r_1,t)) \\ \mathrm{x}\frac{1}{3}(u_1(r_2,t+\tau) + u_2(r_2,t+\tau) + u_3(r_2,t+\tau))\Big] \tag{2.62}$$

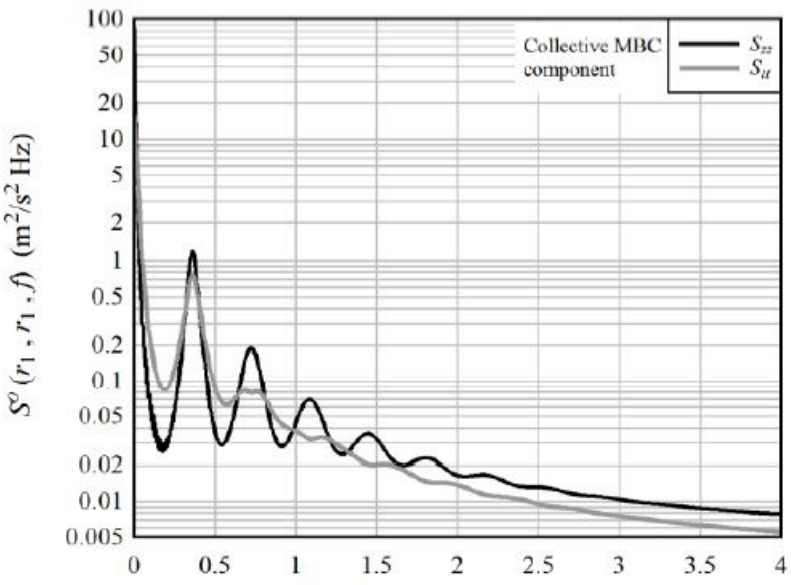

Figure 2.7: Wind spectrum for the collective components in MBC. The x-axis is frequency in Hz (in courtesy of Merz [2015a]).

A more thorough explanation of the translation from the single point spectrum to cross-spectra in MBC can be obtained in Merz [2015a], where the equations from (2.58) to (2.62) are collected from.

2.4 Superposition

Now, both the relations between wind and thrust force, and excitation force and motion of the SSWT are established. Therefore it is possible to superpose the solution to obtain a spectral formulation for the SSWT subjected to both wind and wave forces.

The total force can be written as Equation 2.63. Where the force from wind has been transformed into the global coordinate system, applied as a force in x-direction, and a pitching moment.

$$\mathbf{F}(\omega) = \mathbf{F}_{\zeta}(\omega) + \mathbf{F}_{U}(\omega) \tag{2.63}$$

Now the total motion spectrum for dynamic response analysis for SSWT subjected to wind and wave can be obtained as below. Subscript denotes force-direction, where 1 is surge motion/force in x-direction, 3 heave/force in z-direction and 5 pitch/moment about y-axis. The superscript denotes "2nd" for contribution from second order loads, and "u" for contribution from the thrust force on the rotor. The total motion spectrum is then a summation of the contribution of the 1st order wave loads, the second order wave loads and the global transformation of the thrust force. Respectively in Equation 2.54, 2.65 and 2.66, for surge, heave and pitch motion.

$$S_{Y_1Y_1}(\omega) = |H_{\zeta Y_1}(\omega)|^2 S_{\zeta\zeta}(\omega) + |H_{FY_1}(\omega)|^2 S_{F_1^{2nd}F_1^{2nd}}(\omega) + |H_{FY_1}(\omega)|^2 S_{F_1^{u}F_1^{u}}(\omega) \tag{2.64}$$

$$S_{Y_3Y_3}(\omega) = |H_{\zeta Y_3}(\omega)|^2 S_{\zeta\zeta}(\omega) + |H_{FY_3}(\omega)|^2 S_{F_3^{2nd}F_3^{2nd}}(\omega) \tag{2.65}$$

$$S_{Y_5Y_5}(\omega) = |H_{\zeta Y_5}(\omega)|^2 S_{\zeta\zeta}(\omega) + |H_{FY_5}(\omega)|^2 S_{F_5^{2nd}F_5^{2nd}}(\omega) + |H_{FY_5}(\omega)|^2 S_{F_5^{u}F_5^{u}}(\omega) \tag{2.66}$$

Chapter 3

Procedure

This chapter will go into detail on how the objective of the master thesis is performed. It will document how the results has been achieved, and give knowledge to the process on how the methodology is applied. In Section 3.1 the design will be introduced. This includes both a description of the 5MW NREL wind turbine, the WindFloat hull, and a detailed description on how the load-cases are determined. Following, in Section 3.2, the procedure on how the aerodynamic and hydrodynamic modelling has been conducted is elaborated. Then an insight to the script written for post-processing the results are described in Section 3.3. Finally, in Section 3.4, the FD-model is verified by comparison with TD-simulations. This section includes a short introduction to the theory applied in SRA, and draw the lines on how WindFloat is modelled according to this. Then the configuration for the simulations in TD are listed.

3.1 Design

In this section the design that is applied when establishing the frequency domain method is presented. The wind turbine is a 5MW reference wind turbine developed by Jonkman et al. [2009] for design of offshore wind concepts. A short introduction of it follows in Section 3.1.1. The foundation is a floating semi-submersible design, a modified WindFloat

concept presented in Section 3.1.2. An outline of these designs are presented here, in order to get an idea of the dimensions and capacities of the semi-submersible wind turbine. More detailed information can be obtained through the listed references. Finally a set of environmental load cases are proposed in 3.1.3.

3.1.1 Wind Turbine Design

The design is a 5MW NREL turbine, developed by Jonkman et al. [2009] for conceptual development of offshore renewable energy. This design has been used for several studies, which makes it possible to compare the results with other concepts. The turbine is developed by investigating available information on the market from other wind turbines. Data has then been estimated and analyses has been performed in FAST in order to verify the design. The main properties of the NREL turbine are listed in Table 3.1, consisting of the main dimensions, rated power et cetera. A complete description of the design can be obtained in Jonkman et al. [2009].

Table 3.1: Properties of the NREL Turbine (in courtesy of Jonkman et al. [2009]).

Description	**size**	**unit**
Rated power	5	MW
Rotor Diameter	126	m
Hub Diameter	3	m
Hub Height	90	m
Cut-in Wind Speed	3	m/s
Cut-out Wind Speed	25	m/s
Rated Wind Speed	11.4	m/s
Cut-In Rotor Speed	6.9	rpm
Rated Rotor Speed	12.1	rpm
Rated Tip Speed	80	m/s
Rotor Mass	110 000	kg
Nacelle Mass	240 000	kg
Tower Mass	347 460	kg

For the purpose of achieving the external forces, the turbine is considered rigid, i.e. the turbine and blades are restrained from large deflections. Moreover, the tower is considered fixed both at the bottom of the tower and the top of the tower, so that it will not move due to the external loads.

3.1.2 WindFloat Design

The semi-submersible wind turbine, as shown in Figure 3.1, is a modified WindFloat design. The submerged structure consists of three columns with a diameter of 10m, with attached heave-compensating plates at the bottom of each column in order to reduce heave-motions. The columns are connected by braces. The structure has a ballasting system, in order to decrease the rotations and keep the turbine in upright position to avoid overturning moment. The SRA-model of the FWT is developed by Kvittem [2014]. The floater is moored to the seabed with 4 mooring lines. Two of them are connected to the column where the turbine is attached, and then there is one on each of the two other columns. Some key properties of the WindFloat design are listed in Table 3.3.

Figure 3.1: WindFloat model (in courtesy of Bachynski [2015b]).

Figure 3.2 show the centre of gravity (COG) of the SRA-model. The active ballasting system is altered depending on the mean wind speed at the rotor hub, and this is implemented in SRA by altering the platform inertia and COG as a function of wind speed. Example for one load case with no wind, one above rated and one below rated is given in Table 3.2.

The damped natural periods for the structure can be important to consider when estab-

Table 3.2: How the COG and inertia is altered when ballasting the turbine to avoid steady pitch angle at a mean wind speed. The data below only accounts for the hull, hence turbine and mooring lines are not included (in courtesy of Bachynski [2015c]).

$\bar{U}_{HUB}$ [m/s]	COGx [m]	COGy [m]	COGz [m]	Ixx [Mg*m^2]	Iyy [Mg*m^2]	Izx [Mg*m^2]	Izz [Mg*m^2]
0	-4.300	0.0	-7.937	1.974E+06	1.523E+06	8.829E+04	2.746E+06
8	-5.200	0.0	-7.733	2.012E+06	1.465E+06	1.127E+05	2.746E+06
18	-5.239	0.0	-7.723	2.013E+06	1.462E+06	1.138E+05	2.746E+06

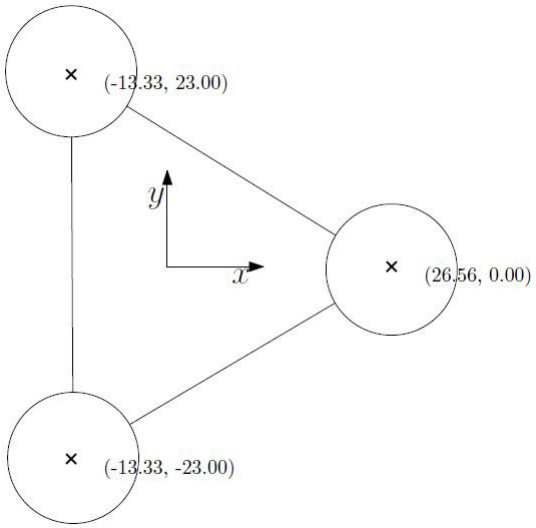

Figure 3.2: COG for the columns in XZ-plane (in courtesy of Kvittem [2014]).

Table 3.3: Properties of the WindFloat design (in courtesy of Kvittem [2014]).

Description	
Displacement with WT	4 810 000 kg
Mass with WT	4 619 000 kg
Mass	4 019 000 kg
COG with WT	(0.331 m, 0.000 m, 1.489 m)
Draught	17 m
Diameter columns	10 m
Diameter horizontal braces	2 m
Z-coordinate COG horizontal braces	-15 m

lishing a frequency domain method, the estimated periods are listed in Table 3.4.

Table 3.4: Damped natural period for WindFloat (in courtesy of Kvittem and Moan [2015]).

Motion	Natural period
Surge	107.0 s
Sway	124.8 s
Heave	19.9 s
Roll	35.6 s
Pitch	37.4 s
Yaw	68.5 s

3.1.3 Loading Conditions

A proposal for initial load cases that the SSWT should be subjected to is presented here. The work is based on the paper that was summarized in Section 1.2.1, all formulas and fittings are obtained from Li et al. [2015]. This section comes with a proposal on how to select the load cases for this project based on the distributions acquired in Li et al. [2015].

The marginal distributions in Li et al. [2015] are based on the wind speed at 10m elevation from the sea surface. For wind, the mean wind speed is assumed to follow the power law profile in Equation 3.1. The exponent is set equal to 0.1. For application on wind turbines it is of interest to apply the wind speed at the hub-height. This can easily be extracted from the relation in 3.1, so that the results from the distributions is represented for mean wind speed at hub-height. The joint distribution for wind speed, wave height and wave period can be used to determine the probability of occurrence for the different variations of these variables. This can for example be used for calculation of fatigue life. With three variables the amount of combinations available is vast, so for the purpose of this thesis it is of interest to reduce the number of load-cases. Therefore the load-cases are determined to be the deterministic most probable significant wave height and peak period based on a given wind speed. Three wind speeds are selected, one below rated, one above rated and one extreme value.

$$U(z) = U_{10}\left(\frac{z}{10}\right)^{\alpha} \tag{3.1}$$

The marginal distribution of the mean-wind speed is described by a two-parameter Weibull

distribution as given in Equation 3.2. The distributions were fitted by applying the maximum likelihood method.

$$f_{U_w}(u) = \frac{\alpha_U}{\beta_U}\Big(\frac{u}{\beta_U}\Big)^{\alpha_U - 1} exp\Big[-\Big(\frac{u}{\beta_U}\Big)^{\alpha_U}\Big] \tag{3.2}$$

The wave height is described by lognormal and Weibull distributions. For each site, a limit for the wave height , h, describes where the lognormal distribution ends and the Weibull distribution begins. However, when selecting the parameters based on a given wind speed it is more interesting to look at the joint distribution of significant wave height, h_s, for a given wind speed, U_w. This distribution is given by a two-parameter Weibull-distribution as seen in Equation 3.3.

$$f_{H_s|U_w}(h|u) = \frac{\alpha_{HC}}{\beta_{HC}}\Big(\frac{u}{\beta_{HC}}\Big)^{\alpha_{HC} - 1} exp\Big[-\Big(\frac{u}{\beta_{HC}}\Big)^{\alpha_{HC}}\Big] \tag{3.3}$$

Then the peak period, T_P, can be determined from the lognormal distribution of peak period for a given significant wave height as given in Equation 3.4.

$$f_{T_P|H_S}(t|h) = \frac{1}{\sqrt{2\pi}\sigma_{LTC}t} exp\Big[-\frac{1}{2}\Big(\frac{ln(t) - \mu_{LTC}}{\sigma_{LTC}}\Big)\Big] \tag{3.4}$$

The load cases are then as given in Table 3.5. Note that the extreme condition has a return period of 50 years, and are the results from Li et al. [2015], for maximum probable wind speed. While the below rated and above rated values for significant wave height and peak period are calculated from Equation 3.3 and 3.4. Although it is common to apply JONSWAP spectrum for this selected site, application of this for these load cases are questionable. A guideline for application of JONSWAP spectrum requires to fulfil the following condition, $3.6\sqrt{H_s} < T_P < 5\sqrt{H_s}$, which is not satisfied for any of the load cases, caution is therefore advised.

Table 3.5: Loading conditions for analyses.

Condition	Mean wind speed	Significant wave height	Peak period
1. Below rated	8 m/s	2.2 m	10.8 s
2. Above rated	18 m/s	4.2 m	11.9 s
3. Extreme	42 m/s	13.4 m	13.1 s

3.2 Modelling

It is important to create a model that in the best manner can represent the true behaviour of the structure. Knowledge to the software is important, and modelling strategies to select correct properties and complexity of the structure. Having routines for verifying a model is beneficial as the output is often a large amount of data. For both the 5MW NREL reference turbine and the WindFloat concept several of studies on these designs are available for comparison when creating the model. In Section 3.2.1, the aerodynamic model of the 5MW NREL turbine is presented. The hydrodynamic panel model is presented in Section 3.2.2.

3.2.1 Aerodynamic model

The aerodynamic model is a state-space model as described in Section 2.2.2, and were provided from Karl Merz. The model is of the 5MW NREL turbine on a bottom fixed OC3 Monopile foundation. As the foundation is not WindFloat, modifications has been made to adjust for this. From the state-space model, only the external forces from wind are acquired, while the motion transfer functions are obtained from analysis in Wadam. This yields that the external forces from the State-Space model must be transformed into the global coordinate system used in the hydrodynamic model. The wind turbine is therefore assumed to be completely rigid. The consequence to this is that there will be no flexibility of the blades, which means that the damping-effect of the motions is lost. This will most likely not be critical for the FD-method, since the motions in the wave frequency-range are inertia dominated. The forces that are subjected to the rotor, contributes most to the pitch motions, and the natural period in pitch is in the low-frequency range. The motions

in the low-frequency range are excited by difference-frequency forces, so if the magnitude of the motions are extreme in this area, it would be recommended to see if the damping from the rotor could contribute to decrease this.

The node in the top of the tower, hence, aligned with the centre of the rotor, is considered fixed. In this way no energy from the external force from wind is lost in the translation to the global coordinate system. This might be a conservative assumption, but the transformation will then become easy, as simple node equilibrium can be used to transform the thrust aerodynamic forces.

3.2.2 Hydrodynamic model

The hydrodynamic loads have been obtained through modelling the submerged part of WindFloat in GeniE, running analysis using Wadam potential solver in HydroD and post-processing the results in PostResp and MATLAB. In this section the details of the procedure of establishing the panel model in GeniE will be presented. Difficulties that are met, some of the assumptions that are made and state the reason for choices that are made will be thoroughly explained, in order for others to be able to reproduce the results.

Establishing the Panel Model

The hydrodynamic loads can be separated into the linear hydrodynamic loads, and higher order hydrodynamic loads. When establishing a frequency domain method it is given that the relation has to be linear, therefore it is necessary to linearise the higher order hydrodynamic loads. Marit L. Kvittem has completed a Ph.D. Thesis on the modified WindFloat design, Kvittem provided the model of WindFloat in HydroD and for application in SRA. The model in HydroD is a combined model described by the panel method (solution based on potential flow theory) and Morison-model. Transfer functions were then obtained by running a Wadam analysis in HydroD, but only the 1st order loads were then accounted for. It was of interest to include some effects due to 2nd order loads, but as known, not all can be achieved when operating in the frequency domain. It is however partially accoun-

ted for by simplified methods where 2nd order loads can be derived from the 1st order potential. From the Wadam analysis, it is possible to obtain the sum-frequency loads, difference-frequency loads and mean drift forces. The mean drift loads can be obtained by a regular Wadam analysis. The sum-frequency and difference-frequency on the other hand, requires a 2nd order free surface model in order to perform the analysis. According to DNV [2011] the 2nd order free surface has to satisfy some requirements; the outer boundaries must represent a perfect circle, the radius of this circle must at minimum be the maximum wavelength of the sea-state and the surface should have a dummy hydro pressure load case. Final demand is that the discretization of the free surface should be established with 4-node shell elements.

In order to determine the maximum wavelength, data from Li et al. [2015] were used. Here the maximum peak period for 50-year condition were given as 14.5 seconds. From the Equation 3.5 (from Faltinsen [1993]) the wavelength assuming infinite water depth is obtained.

$$\lambda = \frac{g}{2\pi} T^2 = 328m \tag{3.5}$$

In order to have a consistent mesh between the boundaries of the structure and the 2nd order free surface a complete description of the structure and sea surface had to be modelled in GeniE. The provided model from Kvittem was not possible to use due to that only the FEM-file was available. The structure was then regenerated in GeniE, with consistent coordinates as used previously in HydroD. The mesh was generated for the combined structure with surrounding sea surface, so that the boundaries were consistent. HydroD requires that the structure and the free surface is imported as separate FEM-files, therefore, when a sufficient mesh was obtained, the mesh-boundaries were locked and then surface was erased and structure meshed in order to get the FEM-file for the structure. Then the structure was erased and the surface was re-meshed. Problem occurred with the 2nd order free surface due to the condition of having only 4-node shell elements, this is difficult to obtain at circular surface with circular cut-outs for the penetrating structure. To ease the process the meshing-rules were edited in order to not allow triangular elements,

and not to alter the number of elements as described by the feature-edges. Feature edges were an important tool in order to get a sufficient mesh, the mesh density close to the structure is larger and then decreasing as the distance from centre of the surface increase as shown in Figure 3.3.

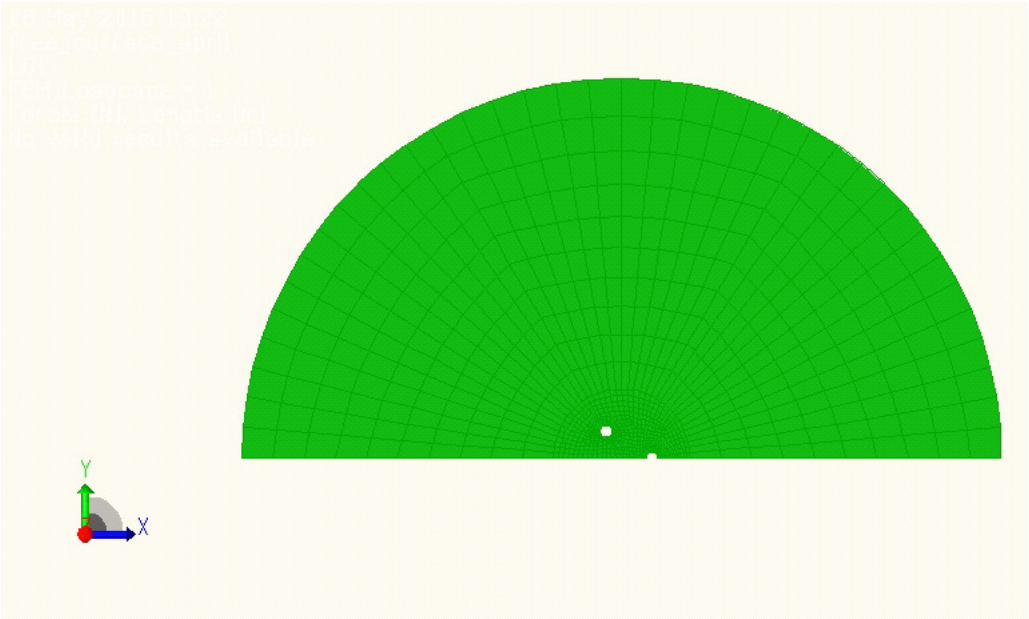

Figure 3.3: The mesh of the second order free surface.

The mesh of submerged part of the structure is presented in Figure 3.5 and 3.4. From the latter figure it is possible to see that the diagonal braces that are in the WindFloat design (Figure 3.1) are not present, this is due to that the dimensions of the diagonal braces are smaller than the other dimensions, consequently it is assumed that they will not contribute significantly to the hydrodynamic loads on the structure. Moreover, it is of interest to reduce the complexity of the structure when performing analysis by use of potential flow solvers, as the computational time increase with number of panels. The heave compensating plates on the bottom of each column are also given an exaggerated thickness, and the mesh is restricted to have two elements over the height in order to calculate the drag forces that are present on these.

When running analysis in HydroD there is also limitation to number of panels in the FEM-file, for the structure this limit is set to 15 000 panels, while for the 2nd order free surface the limit is 3 000 panels. In order to reduce the computational time, symmetry about the

XY-plane is used in the panel model. Since it was incredibly time-consuming to get a mesh in GeniE that did not contain any triangular elements, and since it is very time consuming to calculate the 2nd order forces in Wadam, no mesh convergence test has been performed for the 2nd order free surface. The surface file was however restricted by the limitation of panels, and the final surface contained 897 panels, which is assumed to be sufficient. Both due to that it is close to the limit of allowed number of elements, and since the structure has a finer mesh than the one previously used. The details on number of panels that the final model had, and the restrictions set by Wadam are listed in Table 3.6.

Table 3.6: Overview of the number of panels used to model the WindFloat Platform and the 2nd order free surface, and the maximum allowed number of panels set by HydroD.

Part	**Number of panels**	**maximum allowed**
Structure	12 108	15 000
Free surface	1 794	3 000
Total	13 902	15 000

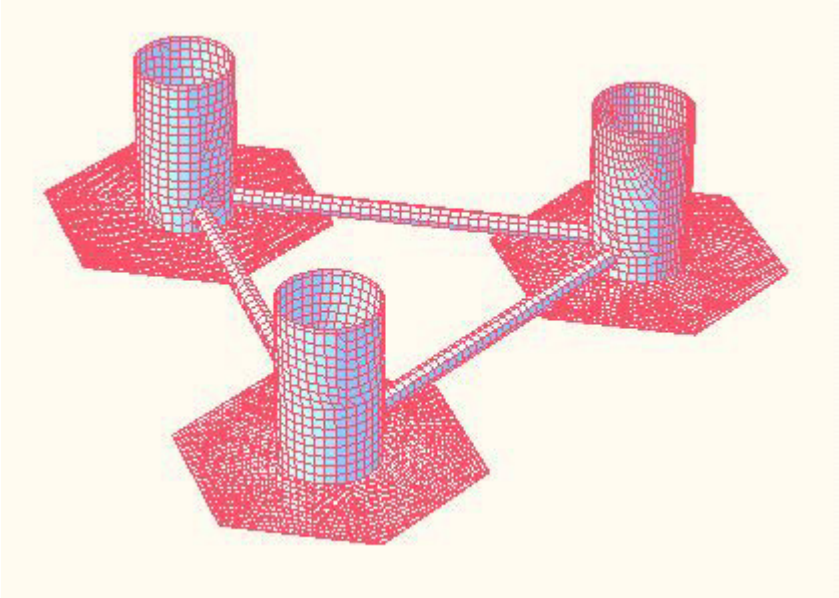

Figure 3.4: Mesh of submerged part of the structure.

These FEM-files were used in order to run the Wadam analysis in HydroD to obtain the difference-frequency effects. For the SSWT, which has large inertia and catenary mooring lines, it is primarily the difference-frequency loads that are of interest due to that the structure has high natural periods that can be excited by difference frequencies. Sum-

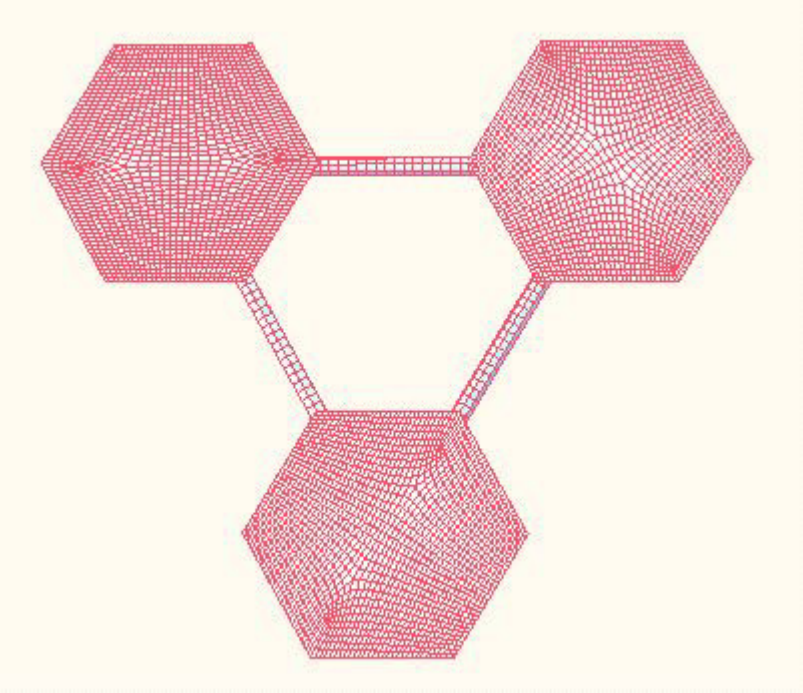

Figure 3.5: Bottom view of the submerged part of the structure.

frequency effects are more interesting when investigating e.g. a TLP, which has low natural periods due to the high stiffness contribution from the a taut mooring system. Therefore only difference-frequency effects were involved in further investigation.

3.3 Post-processing

The overall objective of modelling the submersed part of the structure and running analysis in HydroD is to obtain the transfer-functions that can be applied in the FD-method. Transfer functions for both first order forces and 2nd order difference-frequency forces are obtained through running the potential theory solver, Wadam, in HydroD, and the important aspects around this process is presented in Section 3.3.1. It is possible to post-process the results from Wadam in PostResp (A different module of SESAM), however it is tedious work to export from this program, so a post-processor constructed in MATLAB has been used instead. In addition, creating a post-processor of your own gives more control of the data and greater opportunity to develop additional processing of the data. Through-

out making the post-processor in MATLAB, where it was feasible, the results obtained has been compared to those presented in PostResp. This was done in order to minimize the probability of personal error. The methods applied in the post-processor are summarized here. The overall purpose of the work presented here is to obtain the load and motion spectrum for the hydrodynamic loads.

The results obtained from HydroD and SRA are postprocessed in MATLAB, Figure 3.6 shows an overview of how the work-flow is performed in MATLAB for the hydrodynamic part of the problem. In Figure 3.7, the work flow in the STAS-method is presented. The binary files could not be loaded into MATLAB, and therefore OCTAVE were used to load the necessary files and export them as .mat files that are compatible with MATLAB. Small alterations had to be made for the code, in order for it to run in MATLAB, which was preferable since the author prefers the MATLAB editor. Following in this section is details on how some of the calculations are performed in these scripts, on which method is preferred for obtaining the final results.

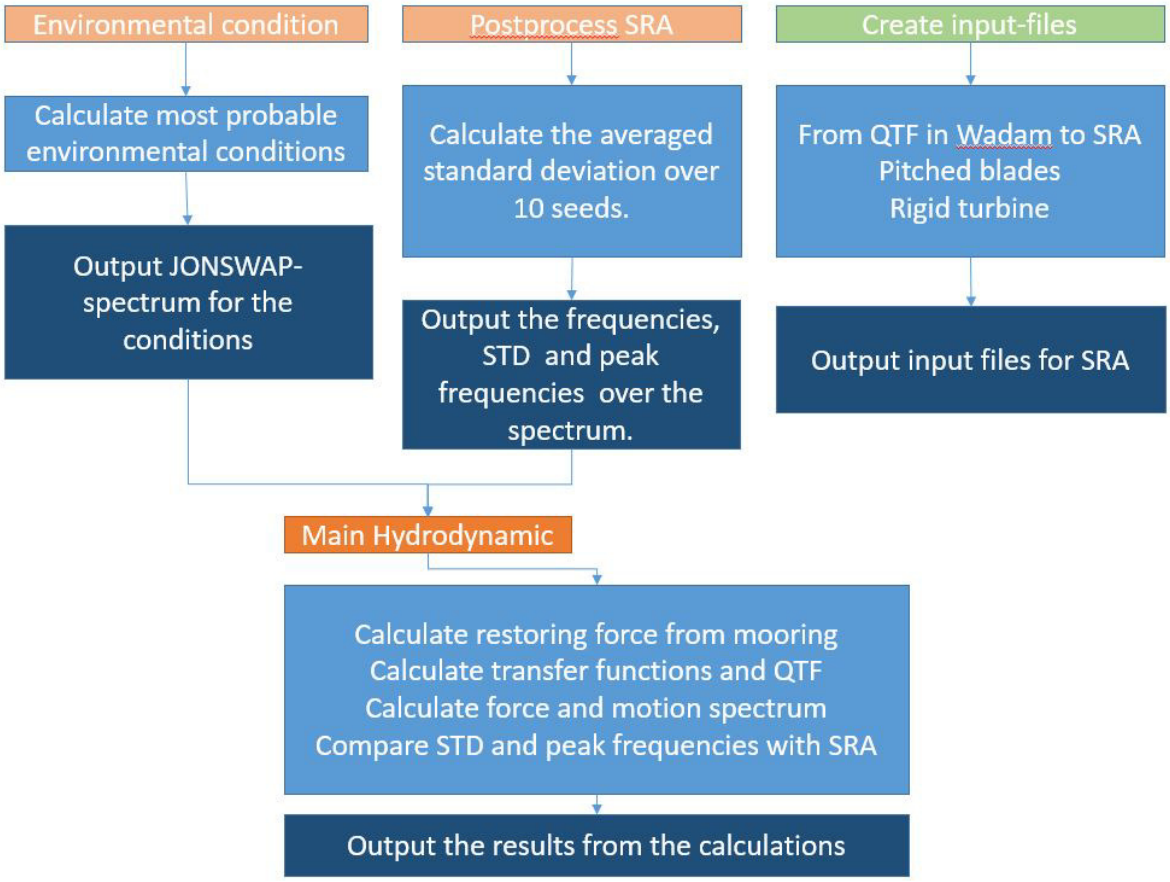

Figure 3.6: Overview of the post-processing of the hydrodynamic data.

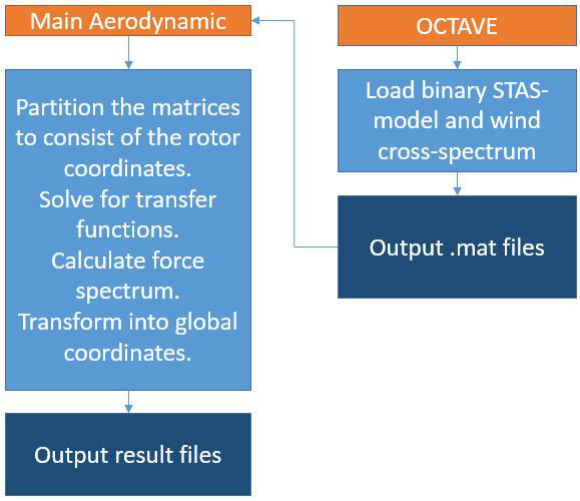

Figure 3.7: Overview of the post-processing of the Aerodynamic data.

3.3.1 Obtaining Transfer Functions for the Hydrodynamic Loads

The FEM-files that were described in the previous section were imported into HydroD in order to obtain the transfer functions for the hydrodynamic loads. The interface in HydroD was for this application used to define the environment, import the FEM-files and customize the calculation details for running the analysis in Wadam. The output from the analysis provides the complex transfer functions in order to establish the dynamic equation of motion for the structure subjected to wave-loads.

The model in HydroD is a dual model, which means that it is both a panel model and a Morison model applied to the same structure. The Morison model is provided by Marit L. Kvittem along with the configuration of the initial panel model and environment in HydroD. The dual model interacts in following way. The panel model computes the pressure distribution from potential flow theory and transfers the results to the Morison model, which has a structural beam representation of Morison elements in 2D and 3D. From Morison equation viscous damping is included, while from the potential flow solution, forces connected to added mass and potential damping are computed.

The simulation is ran for wave frequencies in the range of 0 to 3 rad/s to obtain the linear transfer functions. When selecting the frequencies it is important to include the natural frequencies of the structure (from Table 3.4), since resonance motion occurs there, the largest amplitudes at the transfer-functions are present at these frequencies.

When obtaining the quadratic transfer function (QTF), these effects are only present for the low frequencies, therefore only frequencies from ≈ 0 to 1.3 rad/s are considered. In order to capture the slowly varying motions for the difference frequency effects it is important to have a sufficiently small frequency-interval. This can be determined from looking at the highest natural period, which is the natural period in surge (from Table 3.4), and select a frequency interval that is smaller than the corresponding frequency for this period as shown in Equation 3.6. From this the interval when solving for the QTF's is set to $\Delta\omega = 0.05$.

$$\Delta\omega < \frac{2\pi}{T_{N1}} = 0.06 \tag{3.6}$$

The catenary mooring system is not modelled in HydroD. The mooring lines contributes to horizontal stiffness in surge, sway and yaw, therefore it is of interest to add this into the dynamic equation of motion, more specifically in the restoring coefficient matrix. This has been done in a simplified manner, where the motions are assumed to be uncoupled. Then the expression for the dynamic equation of motion can be simplified to 3.7. By applying the natural periods in surge, heave and yaw from Table 3.4, the analysis in Wadam was performed for their corresponding frequencies, so that added mass for that frequency is known. By assuming that the damping term is zero for oscillation at the natural frequency, and setting the force on the right-hand side of Equation 3.7 to zero, it is clear that there has to be a solution where x_{0i} is not zero. This is given by the eigenvalue problem in Equation 3.8.

$$[-\omega^2(M_{ii} + A_{ii}(\omega)) + i\omega B_{ii}(\omega) + C_{ii}]x_{0i} = f_{0i} \tag{3.7}$$

$$(C_{ii} - \omega_{n,i}^2 M_{ii} + A_{ii}(\omega_{n,i})) = 0 \tag{3.8}$$

Where $i = 1,2,..6$ and the frequency is the natural frequency for degree of freedom number i, the mooring line stiffness is found by solving for C_{ii} in Equation 3.8, and inserted in the global stiffness matrix, **C**.

The results from HydroD are only considering waves propagating in the x-direction, consequently there is not much forces excited in yaw, sway or roll. Thus, the results presented later on are only considering surge, heave and pitch motion.

3.3.2 Integrating the Second Order Force Spectrum

As was presented in Section 2.1.3, second order force spectrum in Equation 2.34 is obtained by substituting the frequency variables and integrating over infinity. The output in Wadam is however limited to a frequency range with positive and negative difference-frequencies with a constant spacing, $\Delta\omega$. The second order force spectrum must therefore be solved by numerical integration. The symmetry relations from Equation 2.23 are applied to generate a one-sided spectrum. Equation 2.34 is then rewritten as Equation 3.9.

$$S_{F_2F_2}(\omega_j) = 2\sum_{i=1}^{N} |H_2(\omega_j + \mu_i, \mu_i)|^2 S_{\zeta\zeta}(\omega_j + \mu_i) S_{\zeta\zeta}(\mu_i) \Delta\mu \tag{3.9}$$

3.4 Verification

In order to verify the quality of the FD-method that is established, comparison to TD-analysis is necessary. When running analysis it is important to have an idea on the theory and applications of the software, in order to perform the analysis correctly and give rise to the ability to identify possible errors in the results. This section will give a brief introduction to the numerical methods that fund the basis for SRA in Section 3.4.1. Then the key aspects for the configuration of the WindFloat model for wind-only and wave-only analyses are presented.

3.4.1 Application of SIMO-RIFLEX-AeroDyn

This section is based on Ormberg and Bachynski [2012], Moriarty and Hansen [2005], MARINTEK [2012a] and MARINTEK [2012b]. A brief introduction to the different codes SIMO, RIFLEX and AeroDyn and its applications.

SRA calculates the response by nonlinear time domain analysis. By imposing dynamic equilibrium in every time step, including both dynamics in blade, mooring system, and

the tower motions. The code considers external force from wind, waves and current. AeroDyn is implemented in SRA as a dynamic link library, where the loads are calculated by a finite element method based on displacement, assuming moderate strains of the structure. The dynamic equation of motion is dependent on both time and frequency. Added mass and damping terms are frequency dependent, in addition harmonic loading is dependent on frequency. This is accounted for by retardation functions. Starting with the dynamic equation of motion in time domain, by applying a convolution theorem, Fourier transform and then establish retardation functions to reach the, frequency dependent, linear equation of motion. Retardation functions are applied in the software in order to calculate simultaneous response dependent on both time and frequency. The governing principle is that work done by the external loads shall be equal to the work absorbed by the structure, this include dissipative, inertial and internal forces. Structural damping is applied by Rayleigh damping, which assumes that the damping is proportional to the mass and stiffness matrices of the dynamic equation of motion. Proper selection on the weighting parameters ensures that the damping is not overestimated.

Time integration is performed by Newmark-Beta, which is an implicit method for iteration. This method can weight the importance of the acceleration and velocity in the current time-step, when estimating the next time-step. Newmark-Beta in this way is capable of both calculating a system with no damping, a system that has negative damping, or artificial damping, by altering the Beta-parameter.

For load histories with bifurcation, limit points and turning points, proper description of the load-displacement history is ensured by the Newton-Raphson method. This method provides iteration within a time-step, and alters the tangential stiffness matrix in order to converge towards equilibrium between the load and displacement.

SIMO:

The large volume structures are modelled as SIMO-bodies. This includes the nacelle, the columns and heave-compensating plates in WindFloat. Loads on these elements are calculated based on linear potential forces (for the frequency dependent terms). Second order forces included are mean drift forces and viscous drag forces. The mean drift forces,

are either based on 2nd order potential forces or 2nd order transfer functions. The drag forces are proportional to the velocity squared. Gravity and buoyancy forces are included by hydrostatic stiffness. SIMO also generates the wave spectrum and current. Wind can also be generated by SIMO, but when using SRA, wind-input from SIMO are dummy variables.

RIXLEX:

Slender body elements are modelled as RIFLEX elements. This includes the turbine-tower, the blades, mooring lines, the shaft and the braces on the WindFloat model. For calculating loads on the mooring lines, the impact from elasticity, weight, buoyancy and hydrodynamic loads are included. The calculation of the hydrodynamic loads are based on the Morison load model, which has a mass-dependent term and a drag dependent term. The drag forces include both drag from wind and wave, as well as a representation of drag on mooring lines that includes relative velocity. The drag forces contribute to damping, excitation and response of the system.

The finite element formulation in RIFLEX is based on small strain approximation, which is adequate for application to slender marine structures. Motions are described by lagrange, where bar elements use a total lagrangian description while beam elements use a co-rotated ghost reference. The advantage with the co-rotated ghost reference, is that it requires no transformation of stress or strain. The principle of virtual work equations is based on green strain and symmetric Piola Kirchhoff stress. The volume loads are calculated directly in the global reference system, while other loads are calculated in local element before transformation to the global system.

AeroDyn:

The wind loads are calculated on the blades, the turbine tower and the nacelle. For the tower and the nacelle the Morison model is used, while for the blades AeroDyn gives the option of using BEM or GDW theory, as explained in Section 2.2.1 and 2.2.1. Dynamic stall is accounted for by Beddoes-Leishman method introduced in Section 2.2.1.

3.4.2 Configuration for Wave-only Simulation

For the wave-only simulations, ten 1-hour simulations are averaged for each load-case. The blades on the rotor must be parked, this means that the blades are pitched 90 degrees, to avoid generating lift due to the motion of the hull. In addition, a master-slave connection between the top of the tower and the end of the shaft is imposed. This is in order to ensure that the blades will not rotate. A dummy wind-file must be input, with a infinitesimal low wind velocity and duration at least as long as the simulation. Significant wave height and peak period is then altered depending on the load case. In order to ensure that the wave-seed is not repeating over the 10 simulations in each load case, these are input as different seeds.

The quadratic transfer functions from HydroD had to be implemented in SRA in the sys-file. The format from the output in HydroD is different from the format in SRA. This was solved by extracting the QTF form PostResp and altering the format to the requirements in SRA. In order to compare over the same frequencies in of the TD-simulation and the FD-simulation, these were selected in the OUTMOD-module to print the wave-frequencies applied when generating the sea-surface. This determines the range of the wave-frequencies, while any result below the minimum value would have to be due to a frequency pair, hence difference frequency effect from QTF. This output allows the FD-method and TD-simulation to be compared based on the same frequencies. In addition, the DYN-WFloat.MAC file must be altered to account for the QTF.

In order to verify the result, spectral analysis of the TD-simulation is compared to the one obtained by the FD-method. Standard deviation and peak frequencies are compared. These parameters are calculated for every seed, and then averaged. Every seed has a frequency-set, and this is applied to the FD-spectrum in order to interpolate the spectrum for the same frequencies and then the results are averaged. In the spectral analysis the motions can be divided into two domains, the wave frequency (WF) range, where the first order excitation is present, and the low frequency (LF) range where the difference-frequency loads are excited.

3.4.3 Configuration for Wind-only Simulation

Two configurations are present for the wind-only simulations. First, to control whether the state-space model represents the true thrust force the first point on the list below must be used. Then in order to investigate if the FD-method is able to represent the wind-induced motions. The configuration in the second point on the list is applied.

1 The turbine is fixed in the top and the bottom of the tower. This is imposed by constraining supernodes in the top and bottom of the tower. Moreover the tower and the blades are considered rigid, this is imposed by multiplying the stiffness by 100 of its actual value. This is to reduce the deformations, so that the true external force can be obtained and reduce loss due to deformations. Turbulent wind-field generated from a Kaimal spectrum is applied.

2 The SSWT is freely floating, only restricted by the mooring lines. The tower and blades are not rigid. Turbulent wind-field generated from a von Karman spectrum is applied. The QTF, as described in wave-only configuration is included.

The SRA-model of the 5MW NREL turbine and the WindFloat concept was provided by Professor Erin E. Bachynski, and these are modelled by Kvittem [2014]. The application for this project was to alter the geometrical properties and apply the required loading to run the analyses. For both of the configurations the following applies.

For the 5MW NREL turbine BEM is applied up to wind speed of 8 m/s for the turbulent wind simulations. 8 m/s is the limit velocity for where to apply BEM or GDW. By comparing the mean value of thrust and torque for simulations with both BEM and GDW it was observed that BEM is the method that coincides with the curve representing mean force for given velocities. The turbulent wind field consists of velocities both above and below the limit, so BEM was better at representing the higher velocities than GDW was at calculating the lower velocities. For the above rated and extreme condition GDW should be applied.

For turbulent wind simulation dynamic stall is included. A dummy input for significant wave height and peak period is selected so that there is in practice no waves.

Wind-files generated in TurbSim are compatible with SRA. The key properties that must be determined when generating wind files is to select the size of the grid and the grid-spacing, type of spectrum, magnitude of turbulence and wind-shear profile. The most important is to have a grid that is larger than the rotor, and a grid-spacing smaller than the chord length of the airfoil of the turbine. More information of how to use TurbSim can be found in Jonkman [2009]. The grid is described by 32x32 points covering an quadratic area of 160 m^2.

In order to compare the results from the TD-simulation and the ones obtained by the FD-method, a spectral analysis is conducted. By use of WAFO-toolbox (Brodtkorb et al. [2000]) in MATLAB it is simple to generate a spectrum of the timeseries from SRA. Then comparison of the force-spectrum is conducted. Comparison between the standard deviation and the peak frequency indicates the quality of the FD-method. It is important to run sufficiently long simulations in TD and remove the first part of the time-series prior to processing the data. This is due to transient effects in the start-up of the simulation. This can easily be seen when plotting the entire time-series, as the first part of the simulation shows an abnormal behaviour. The simulation is ran for 2000 seconds, where the first 400 seconds are omitted.

Chapter 4

Result

The three load cases (LC) presented in Table 3.5 has been analysed. In this chapter condition 1/LC1 refers to the below rated condition, condition 2/LC2 is above rated, and condition 3/LC3 is the extreme condition from Table 3.5. For the hydrodynamic analyses all three LC has been performed, while for the aerodynamic analyses only LC1 and LC2 are presented. Section 4.1 presents the linear response amplitude operators obtained from HydroD. Next, the mean drift forces are examined in Section 4.2. Then the first and second order force spectra are presented in Section 4.3. Then follows a comparison between the frequency domain method and time-domain analyses in Section 4.4. Finally, the results obtained from the state-space model of the turbine are presented in Section 4.5.

4.1 Linear Response Amplitude Operators

The linear response amplitude operators (RAO) are the absolute value of the linear transfer functions. From Figure 4.1, the natural frequency in surge can be identified for the surge RAO (in Figure4.1a), and also the first peak at the pitch RAO (in Figure 4.1b). The natural frequency in heave is 0.31 rad/s, whereas the peak in Figure 4.2a is at 0.30 rad/s. This is due to that the heave natural frequency was not included in the Wadam analysis.

The velocity and acceleration RAO of the motion are presented in Figure 4.2 and 4.3. By

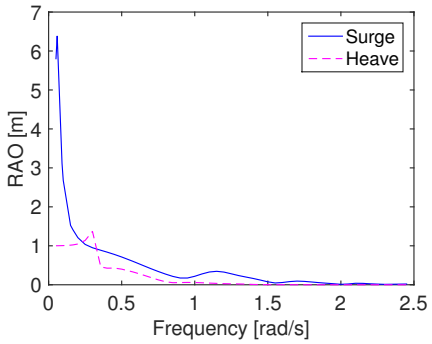

(a) RAO in surge and heave.

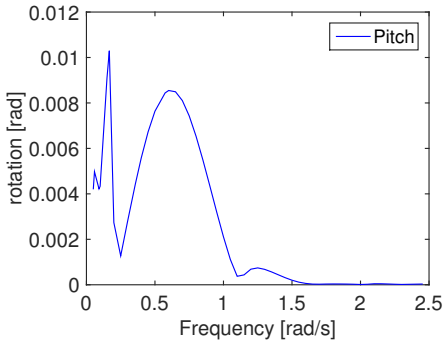

(b) RAO in pitch.

Figure 4.1: Response amplitude operators in surge, heave and pitch.

comparison with the acceleration in Figure 4.3a and 4.3b, the shape of the RAO for surge and pitch has strong resemblance to the excitation force in Figure 4.1. From this relation it is clear that the linear excitation forces on the hull are inertia dominated.

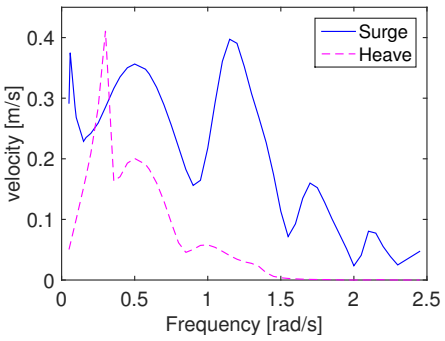

(a) Velocity in surge and heave.

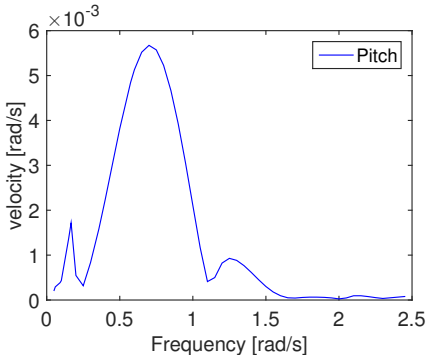

(b) Velocity in pitch.

Figure 4.2: Velocity RAO in surge, heave and pitch.

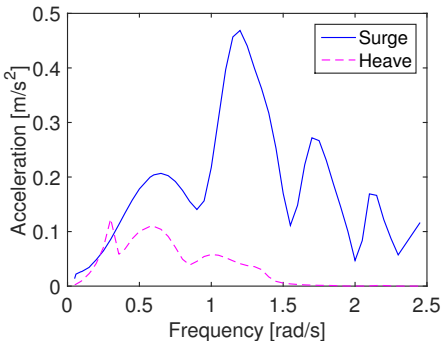

(a) Acceleration in surge and heave.

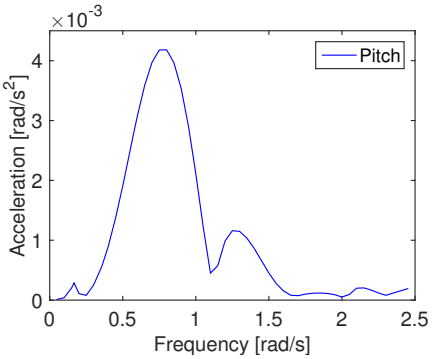

(b) Acceleration in pitch.

Figure 4.3: Acceleration RAO in surge, heave and pitch.

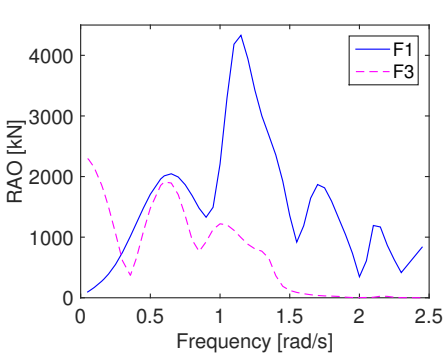

(a) Excitation force in surge and heave.

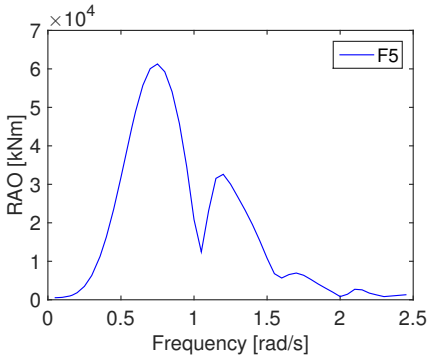

(b) Excitation force in pitch.

Figure 4.4: Excitation forces.

4.2 Mean Drift Forces

The mean drift forces were calculated by pressure integration in six degree of freedom. Heave and pitch is excited by a peak at the natural frequency in heave (ω =0.31 rad/s). The peaks at ω =2.28 rad/s in surge and pitch, coincides with the first tower bending mode. It can be observed by comparing the mean drift forces and the linear wave induced excitation forces, that the mean drift forces are approximately an order of 10 lower in magnitude. An example of the mean drift forces can be seen in Figure 4.5.

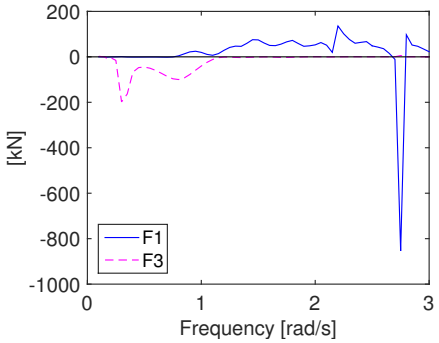

(a) Force in surge and heave.

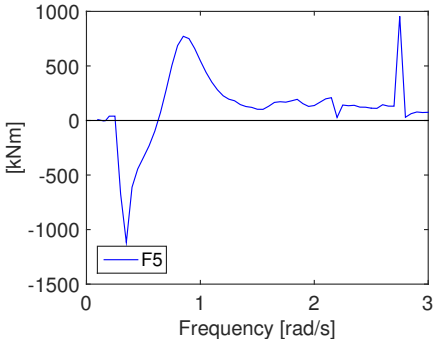

(b) Moment in pitch.

Figure 4.5: Mean drift forces in surge, heave and pitch.

4.3 Spectral Analysis of the Hydrodynamic Force Spectra

In this section the results from the spectral analysis are presented. This includes both the first and second order force spectrum, followed by a more thorough examination of the three load cases and the motion spectrum produced from these. The load case also shows the comparison to simulations in SRA, to evaluate the accuracy of the FD-method.

4.3.1 1st Order Force Spectrum

The first order force spectrum is presented in Figure 4.6 for the three conditions. The linear spectrum has the same shape for each condition, but the extreme condition has significantly higher peak. This then covers a broader range of frequencies, which implies a broader band. This indicates a less Gaussian process for an extreme sea-state. The peak frequency for the different loading conditions are listed in Table 4.1. As seen from the table, the peak frequency shifts towards the left with increased severity of the sea-state. This substantiates that there is more energy present in the LF region, where 2nd order effects are expected.

Table 4.1: Peak frequencies for first order force spectrum.

LC	ω_P **[rad/s]**
LC1	0.60
LC2	0.55
LC3	0.50

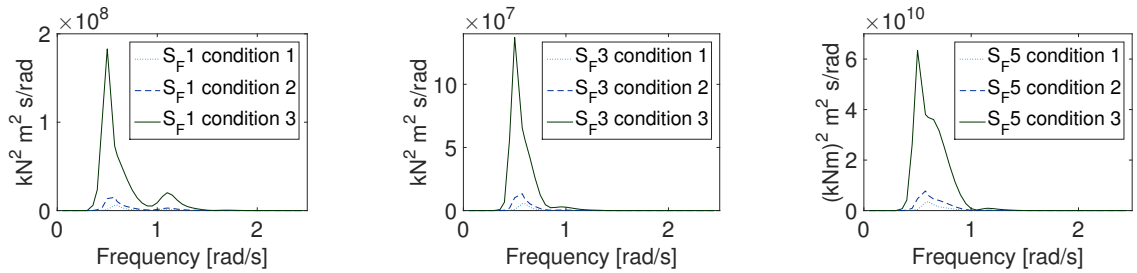

(a) Surge. (b) Heave. (c) Pitch.

Figure 4.6: Force spectrum from linear wave induced loads.

4.3.2 2nd Order Force Spectrum

In Figure 4.7, the plot from the 2nd order force spectrum is displayed, LC1 and LC2 have so low amplitudes in comparison that they are presented again, in Figure 4.8. Physically there are no dynamic behaviour at $\omega = 0$, the reason to why the spectral value is not zero is that these represent the mean drift forces in the QTF, where $\omega_i = \omega_j$. The 2nd order force spectrum is in the order of 10^2 smaller, in comparison to the 1st order force spectrum. The peak frequencies for the different load conditions are presented in Table 4.2. On the contrary to the behaviour in the first order force spectrum, the peak frequency increases with the severity of the sea-state in heave and pitch degree of freedom, while surge is constant. At a closer view of the three conditions in pitch, a small peak at $\omega = 0.15$ rad/s is present in every condition. This frequency is the one closest to the natural frequency in pitch at ω =0.167 rad/s. Comparing load spectrum of the 1st order and 2nd order does however not give much physical insight to the behaviour of the hull. It is more interesting to see what effect the forces have on the motion, in order to weight the effect the 2nd order forces contributes to the dynamic excitation.

Table 4.2: Peak frequencies in 2nd order force spectrum for surge, heave and pitch motion.

LC	**Unit**	**Surge** ω_P	**Heave** ω_P	**Pitch** ω_P
LC1	[rad/s]	0.35	0.30	0.15
LC2	[rad/s]	0.35	0.30	0.30
LC3	[rad/s]	0.35	0.35	0.40

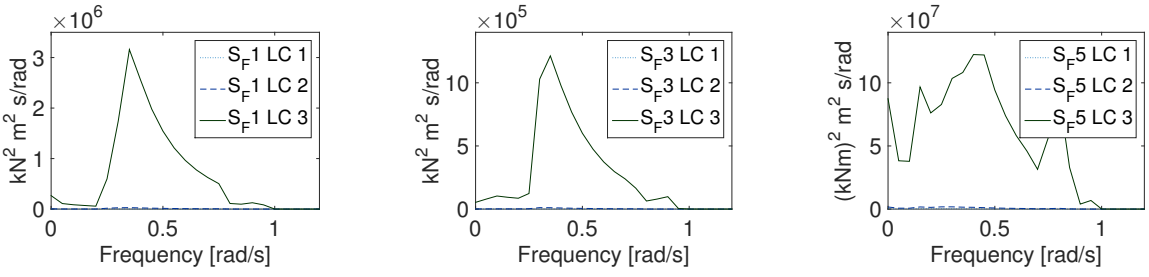

(a) Surge. (b) Heave. (c) Pitch.

Figure 4.7: Force spectrum of second order loads.

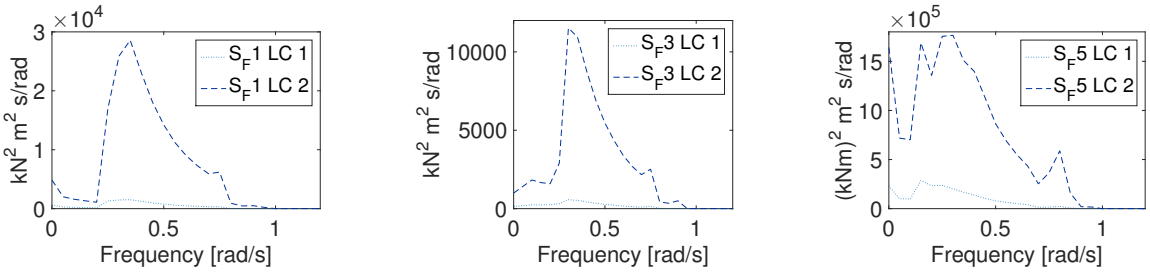

(a) Surge. (b) Heave. (c) Pitch.

Figure 4.8: Force spectrum of second order loads of LC1 and LC2.

4.4 Comparison to Time-Domain Simulations

Following are the results from comparing the motion spectrum of the FD-method and the mean of 10 TD-simulations. The results distinguishes between the WF-region and LF-region based on the frequencies that were output from SRA. The lowest frequency in each output is considered the limit between the WF and the LF-region. Then the LF consists of every possible combination of WF ($\omega_i - \omega_j$) under the condition that they are unique, not negative, and do not exceed the limit into WF-domain. Motion spectra were then interpolated for these frequencies, and the peak-frequencies and standard deviations were compared. In addition the area of the spectra are calculated, thus, the variance. This gives an indication of the validity of the method, as the area is a representation of the energy. In addition, if one of the frequency domains do not give accurate results, it may not be critical to the overall solution. Thus, although the shape may not be equal, if the standard deviation and the area have resemblance this support the FD-method. The areas are calculated as the mean of 10 simulations in SRA for each condition, in FD-approach the area is deterministically constant for each condition. The total areas (including WF and LF) are only calculated for frequencies exceeding 0.1 rad/s of the FD-solution. Thus, the extrapolation of the LF-solution of the FD-method is neglected. The peak frequencies and standard deviation includes the extrapolation. From the tables of the areas that will be presented, it will be possible to see what the error is, if the frequency range below 0.1 rad/s is not included.

4.4.1 Hydrodynamic Results for Load Case 1

Table 4.3 lists the comparison between the peak frequency in the motion specta for load case 1. All of the examined motions show good correspondence in the WF region, with errors below 1%. In the LF region, the same only yields for the peak in heave-motion. The frequencies from TD-simulations for surge and pitch are recognized as approximately the natural period for the corresponding motion. The FD-solution in pitch motion yields the closest value that is proportional with the frequency step, that was applied in acquiring the QTF. The natural period in surge, is lower than the first applicable frequency in QTF ($\omega_i - \omega_j = 0.1$ rad/s). Thus it is clear from Figure 4.9a that the linear extrapolation is not valid.

Table 4.3: Comparison of peak frequencies in FD and TD for WF and LF for load case 1.

		WF			**LF**		
Motion	**Unit**	**TD**	**FD**	**Error**	**TD**	**FD**	**Error**
Surge	[rad/s]	0.579	0.573	1.0%	0.058	0.000	NaN
Heave	[rad/s]	0.575	0.573	0.4%	0.292	0.290	0.5%
Pitch	[rad/s]	0.587	0.585	0.4%	0.164	0.150	9.4%

Table 4.4 lists the comparison between the standard deviation for LC1 for FD and TD-solution. The results in the WF-range yields small errors. While the standard deviation in pitch coincide with the TD-solution, surge and heave overestimates the standard deviation. Figure 4.9a and 4.9b, indicates that the damping is under-estimated as the peaks exceed the TD-solution. In the LF-region, surge has the largest error, from Figure 4.9a the reason why is clear. The extrapolation has no similarities to the true behaviour. The representation prior to the extrapolation coincides quite well with the TD-spectrum.

The standard deviation in heave is underestimated, this area is small in comparison to the other contributions. The LF-area in Figure 4.9c, shows how the pitch motion in FD has a peak prior to the TD-solution, the area is also larger. Thus, if the peak frequency would be correct, it should indicate also underestimated damping in the LF-region.

In Table 4.5 the total variance of the spectra in LC1 are tabulated, in addition to the percentage error between the TD solution and FD-solution. Note that although the only solu-

Table 4.4: Comparison of standard deviation in FD and TD for WF and LF for load case 1.

		WF STD			**LF STD**		
Motion	**Unit**	**TD**	**FD**	**Error**	**TD**	**FD**	**Error**
Surge	[m]	0.286	0.289	-0.9%	0.086	0.875	-90.1%
Heave	[m]	0.148	0.152	-2.4%	0.014	0.009	63.6%
Pitch	[rad]	0.004	0.004	0.0%	0.001	0.002	-13.3%

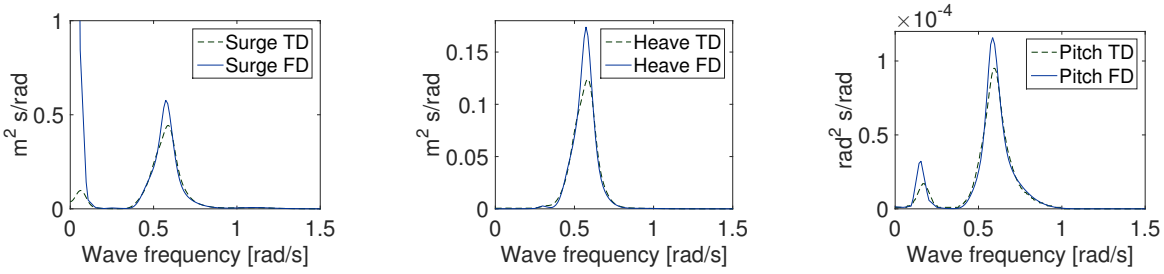

(a) Surge. (b) Heave. (c) Pitch.

Figure 4.9: Comparison between FD-motion spectra and one example of a motion spectrum from TD for LC1.

tion where the transfer functions are extrapolated is included, the frequency domain solution has larger area for all motions.

Table 4.5: Comparison of total area under the spectrum for LC1 when excluding the FD-solution for frequencies below 0.1 rad/s.

Motion	**Unit**	**TD**	**FD**	**Error**
Surge	[m^2]	8.308E-02	8.555E-02	-2.9%
Heave	[m^2]	2.215E-02	2.330E-02	-4.9%
Pitch	[rad^2]	1.800E-05	1.908E-05	-5.7%

4.4.2 Hydrodynamic Results for Load Case 2

In Table 4.6, the comparison of the peak frequencies from TD and FD-method are presented. The WF-region yields small errors for all motions. The LF-region has the same tendencies as in LC1; surge lose the solution due to poor extrapolation, and pitch is as close as possible to its natural frequency with its limitation on being proportional to the applied frequency-step. Heave motion overestimates the peak frequency, but in Figure 4.10b, it is clear that the LF region is infinitesimal with comparison to the energy in the WF-

region.

Table 4.6: Comparison of peak frequencies in FD and TD for WF and LF for load case 2.

		WF			LF		
Motion	**Unit**	**TD**	**FD**	**Error**	**TD**	**FD**	**Error**
Surge	[rad/s]	0.520	0.520	0.0 %	0.060	0.000	NaN
Heave	[rad/s]	0.519	0.520	-0.3%	0.218	0.264	-17.5%
Pitch	[rad/s]	0.535	0.531	0.7 %	0.166	0.150	10.7%

In Table 4.7, the standard deviations for LC2 are presented. The results in the WF-region yields small errors and the standard deviation in pitch coincide with the TD-simulation, as in LC1. From looking at the spectra in Figure 4.10 the peaks in FD- exceed the TD-solution for all motions. However, the standard deviation in heave is a bit underestimated, which is due to the behaviour in the left tail of the spectrum (Figure 4.10b). Again the error of the standard deviations in the LF-region are large. The relative magnitude of the standard deviation, in the LF-domain in comparison to WF-region is quite small. With exception of the surge motion that has unrealistically large values due to the extrapolation, as can be seen from Figure 4.10a.

Table 4.7: Comparison of standard deviation in FD and TD for WF and LF for load case 2.

		WF STD			LF STD		
Motion	**Unit**	**TD**	**FD**	**Error**	**TD**	**FD**	**Error**
Surge	[m]	0.615	0.626	-1.7%	0.228	2.382	-90.4%
Heave	[m]	0.339	0.338	0.3%	0.044	0.018	140.8%
Pitch	[rad]	0.008	0.008	0.0%	0.004	0.004	8.1%

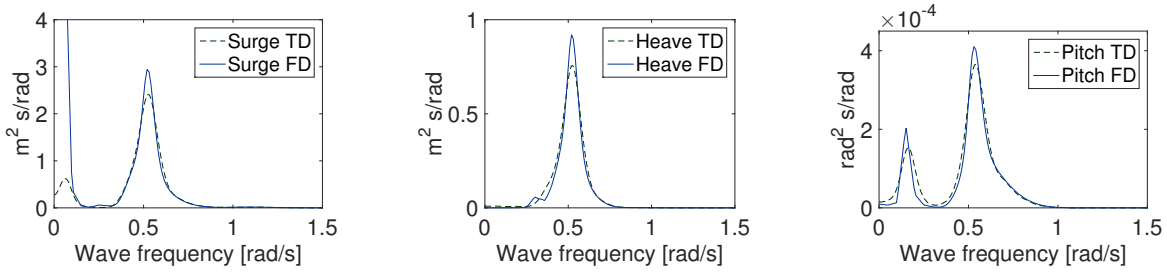

(a) Surge. (b) Heave. (c) Pitch.

Figure 4.10: Comparison between FD-motion spectra and one example of a motion spectrum from TD LC2.

In Table 4.8, the total area of the spectra are tabulated. Note that for the FD-solution, the range where the frequencies are extrapolated are removed. Surge experiences the highest error, but the total area is overestimated.

Table 4.8: Comparison of total area under the spectrum for LC2 when excluding the FD-solution for frequencies below 0.1 rad/s.

Motion	**Unit**	**TD**	**FD**	**Error**
Surge	[m^2]	3.870E-01	4.114E-01	-5.9 %
Heave	[m^2]	1.160E-01	1.183E-01	-1.9 %
Pitch	[rad^2]	7.500E-05	7.370E-05	1.8 %

4.4.3 Hydrodynamic Results for Load Case 3

In Table 4.9, the peak frequencies from TD-simulation and FD-method are listed. The results yields less than 2% error for all motions in the WF-domain. In the LF-domain, the same error that was present in LC1 and LC2 yields for the surge natural frequency. From Figure 4.11b it can be seen that there is some energy in the LF-domain for pitch motion. The representation from TD and FD-solution does however deviate a lot, consequently the peak frequency for heave motion is wrong. Pitch motion has an error of 0.7% as the peak frequency in TD no longer yields the natural period.

Table 4.9: Comparison of peak frequencies in FD and TD for WF and LF for load case 3.

		WF			**LF**		
Motion	**Unit**	**TD**	**FD**	**Error**	**TD**	**FD**	**Error**
Surge	[rad/s]	0.477	0.473	0.9%	0.038	0.000	NaN
Heave	[rad/s]	0.475	0.482	-1.5%	0.064	0.240	-73.5%
Pitch	[rad/s]	0.486	0.483	0.7%	0.151	0.150	0.7%

In Table 4.10 the comparison of the standard deviations for LC3 are listed. Despite that the estimated peak frequency for the motions in FD were quite well represented in WF-region, the error in standard deviation for heave and pitch are almost at 20%. Standard deviation in surge on the other hand, is quite similar to TD-solution. In the LF-reqion the error in surge is quite significant, due to the propagating error caused by extrapolation. Heave motion is poorly represented, and due to the discrepancy that is observed in Figure

4.11b further investigation is advised. The standard deviation in pitch is overestimated by 2.9% by the FD-method. From Figure 4.11c it is clear that the FD-method exceed the magnitude of the TD-method in LF-domain, and vice versa in WF-domain. This shows the importance of including the non-linear forces, as the magnitude of the pitch standard deviation in the LF domain has the same standard deviation as in the WF domain. In Figure 4.11a, there is also a large fraction of the total area in the LF-domain. So this applies also for surge motion.

Table 4.10: Comparison of standard deviation in FD and TD for WF and LF for load case 3.

		WF STD			**LF STD**		
Motion	**Unit**	**TD**	**FD**	**Error**	**TD**	**FD**	**Error**
Surge	[m]	2.196	2.212	-0.7%	1.765	17.626	-90.0%
Heave	[m]	1.452	1.215	19.5%	0.452	0.088	411.2%
Pitch	[rad]	0.028	0.024	18.0%	0.027	0.028	-2.9%

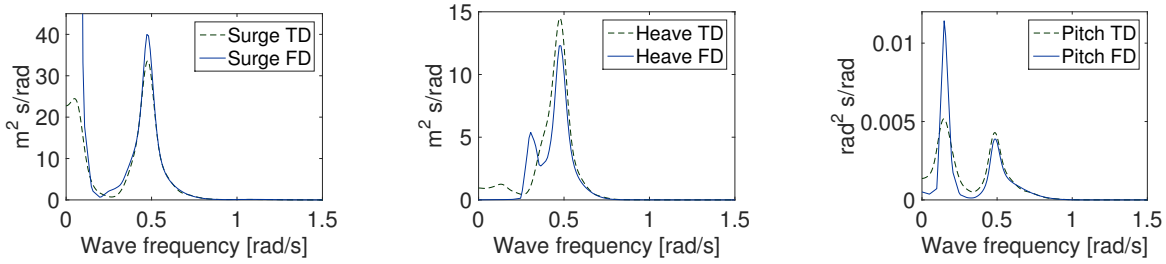

(a) Surge. (b) Heave. (c) Pitch.

Figure 4.11: Comparison between FD-motion spectra and one example of a motion spectrum from TD for LC3.

In Table 4.11, the areas and the percentage error are listed. It substantiates the problem with heave motion, as the area is underestimated by nearly 20%. Surge experiences rather high error also, but the area in the FD-method is larger than the TD method, thus it would most likely give conservative results.

Table 4.11: Comparison of total area under the spectrum for LC3 when excluding the FD-solution for frequencies below 0.1 rad/s.

Motion	Unit	TD	FD	Error
Surge	[m^2]	5.314E+00	6.081E+00	-12.6 %
Heave	[m^2]	2.213E+00	1.855E+00	19.3 %
Pitch	[rad^2]	1.323E-03	1.319E-03	0.3 %

4.5 Spectral Analysis of the Aerodynamic Loads

This section will present the results from the state-space model of the wind turbine. In order to validate the results, the power spectrum for thrust force has been compared towards similar analysis in SRA. The difference is that the SRA-configuration consists of a turbulent wind field from a Kaimal-spectrum, with normal turbulence model (NTM) and turbulence intensity of 0.11. While the wind applied in the state-space model is generated from a Von Karman spectrum, with NTM and turbulence intensity 0.14. The parameter that will be compared is the peak frequencies present in the power spectrum which are deterministically dependent on the rotational frequency of the rotor, that should be independent on type of spectrum. The TD-results are obtained from a simulation of length 1600 seconds (excluding transients).

Due to the presence of the tower, the wind turbine experience vibrations that are proportional to the multiples of the rotational frequency of the rotor. For a three-bladed turbine, these are present as multiples of 3. The significance of these vibrations decrease with increase of n (considering nP). For thrust force, the wind frequencies has most influence on the power spectrum, while the nP-effects are small in comparison. Therefore, the figures presented has a logarithmic scale on the y-axis to see the effects of the vibrations. The rotor and blade-passing frequencies are listed in Table 4.12.

Since condition 3 has a wind-speed above the cut-out wind-speed, the blades are parked and drag forces gives the main contribution from the turbine. Moreover these nP-effects would not be present in a spectral analysis.

Have in mind that the results presented in this section are a comparison between FD-method and one simulation in SRA.

Table 4.12: The rotor blade passing frequencies and its multiples for LC1 and LC2

nP	Unit	LC1	LC2
1P	[rad/s]	0.97	1.27
3P	[rad/s]	2.92	3.80
6P	[rad/s]	5.84	7.60
9P	[rad/s]	8.77	11.40
12P	[rad/s]	11.69	15.21
15P	[rad/s]	14.61	19.01

4.5.1 Aerodynamic Results for Load Case 1

Table 4.13 shows the comparison between the 3P and 6P frequency for LC1 in TD and FD. The FD-solution underestimates the peak by less than 5 %. From Figure 4.12 it is clear that several peaks are present in the FD-solution. However, from the TD-spectrum in Figure 4.13 it can be seen that the exact position of the higher order nP are difficult to determine. When applying a filter to the spectrum, coherence between $\omega = 0$ and 6P were emphasized.

Table 4.13: Comparison between spectral peaks from FD and TD for LC1.

FD [rad/s]	TD [rad/s]	Error [%]
2.86	2.98	-4.09
5.75	5.92	-2.99

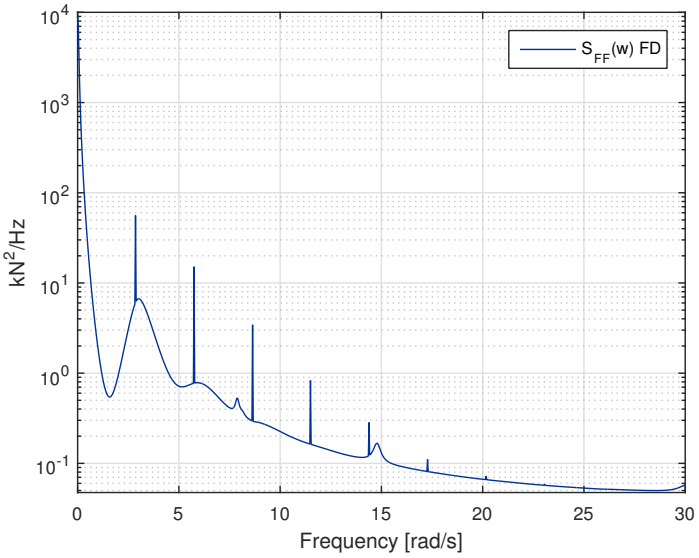

Figure 4.12: Power spectrum for thrust force from FD-method, LC1. One blade, based on von Karman wind spectrum.

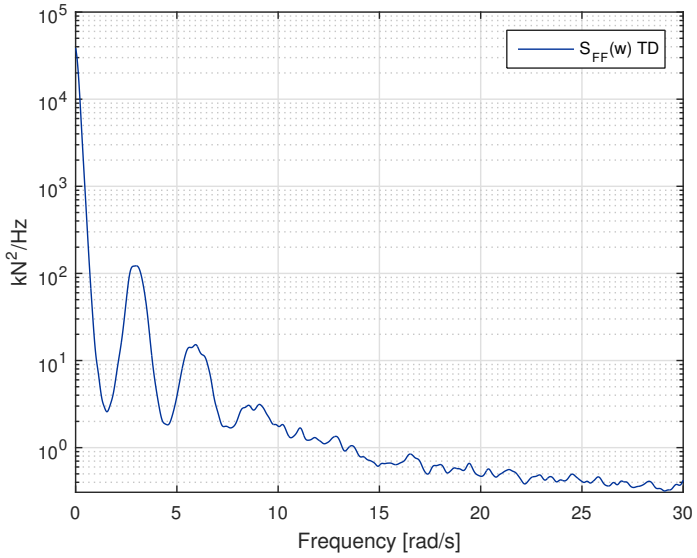

Figure 4.13: Power spectrum for thrust force from TD-simulation of LC1. Based on Kaimal wind spectrum.

4.5.2 Aerodynamic Results for Load Case 2

In Figure 4.15, the power spectrum from the SRA-simulation is presented. From this, the peak frequencies from 3P-15P were obtained and compared towards the FD-spectrum for the thrust force (in Figure 4.14). In Table 4.14, the percentage error between the peak frequencies in the two spectra are listed. The state-space model underestimates the TD-solution by less than 1% in every case.

Table 4.14: Comparison between spectral peaks from FD and TD for LC2.

FD [rad/s]	TD [rad/s]	Error [%]
3.77	3.80	-0.90
7.57	7.58	-0.09
11.37	11.43	-0.53
15.17	15.28	-0.73
18.98	19.04	-0.32

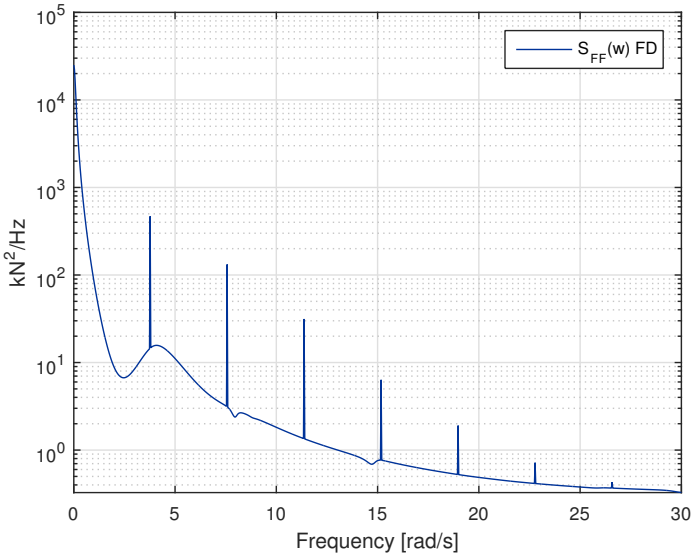

Figure 4.14: Power spectrum for thrust force from FD-method, LC2. One blade, based on von Karman wind spectrum

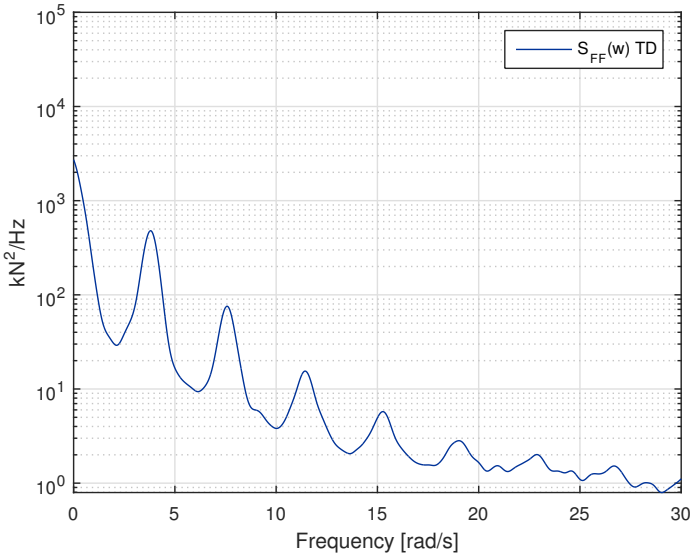

Figure 4.15: Power spectrum for thrust force from TD-simulation of LC2. Based on Kaimal wind spectrum.

4.5.3 Comparison With Blade Passing Frequency

Since the spectrum from the TD-simulations are dependent on how the spectrum is calculated and sensitivity to filtering, the FD-solution is also compared towards the actual rotational frequency. For the 5MW NREL turbine the rotational frequency is increasing up to rated wind speed, and then constant above rated wind speed. The rotational frequency applied here is the mean from each of the two simulations in SRA. The errors are listed in Table 4.15, and the trend is clear, that FD-method has a slight underestimated value, by less than 1% for LC2 and between 1.5% and 2.5% for LC1.

Table 4.15: Comparison of the spectral peaks from FD with multiples of the blade passing frequency of the rotor for LC1 and LC2.

nP	**LC1 error [%]**	**LC2 error[%]**
3P	-2.19	-0.84
6P	-1.64	-0.43
9P	-1.46	-0.31
12P	-1.62	-0.24
15P	-1.52	-0.15

4.5.4 Comparison of Wind Induced Motion Spectrum

The thrust force is transformed into the global motion spectrum and compared towards one simulation in SRA for LC1 and LC2. For this purpose, new wind-files were generated with the same type of spectrum and turbulence intensity as applied in the state-space model.

A comparison of the surge motion spectra for LC1 and LC2 are given in Figure 4.16. The shape of the spectra are quite similar independent on which LC that is investigated. The FD-method is however not capable of representing something that resembles the TD-solution for frequencies that are lower than approximately 0.09 rad/s, in Figure 4.16b. Surge motion in LC1 has a larger offset for following the TD-solution, in the region where LC2 were close to the TD-solution.

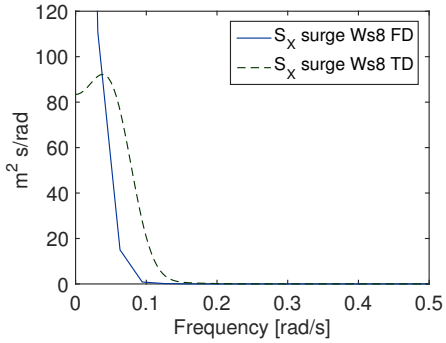

(a) Surge motion with mean wind-speed 8 m/s.

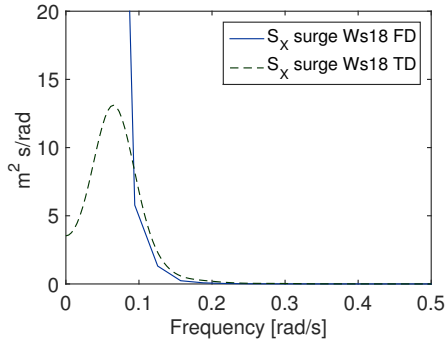

(b) Pitch motion with mean wind-speed 18 m/s.

Figure 4.16: Surge motion spectra for turbulent simulations with mean wind-speed of 8 m/s and 18 m/s.

In Figure 4.17, the motion spectra for pitch motion are presented. LC2 in Figure 4.17b shows better resemblance in comparison with surge motion, but again, the left tail below approximately 0.9 rad/s deviates from the TD-solution. In the better represented area, the TD-solution yields a higher peak and area. In Figure 4.17a, there is no coherence with TD and FD. This emphasize that there is some error with LC1 that has not been detected, since the pitch motion is wrong and the surge spectrum yields much worse result than LC2.

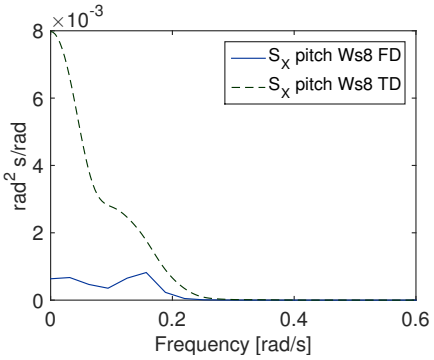

(a) Pitch motion with mean wind-speed 8 m/s.

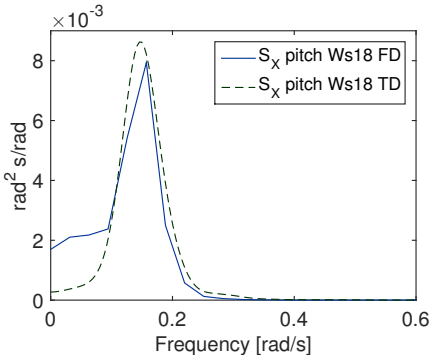

(b) Pitch motion with mean wind-speed 18 m/s.

Figure 4.17: Pitch motion spectra for turbulent simulations with mean wind-speed of 8 m/s and 18 m/s.

In Table 4.16, the standard deviation for the motion spectra are presented. Due to the extrapolation of the surge transfer function, the deviation between TD and FD for surge motion yields large errors. The standard deviation for pitch in LC2 is well represented.

Table 4.16: List of computed standard deviation in TD and FD, for both loading conditions and all motions.

Motion/LC	**Unit**	**FD STD**	**TD STD**	**Error**
Surge LC1	[m]	3.622	2.759	31.3%
Surge LC2	[m]	6.147	1.031	496.0%
Pitch LC1	[rad]	0.011	0.027	-60.5%
Pitch LC2	[rad]	0.028	0.027	0.8%

In Table 4.17, the peak frequencies for the spectra are presented. The peak in surge is zero for both conditions in the FD-solution. The pitch motion on the other hand, has errors below 7% for both conditions.

Table 4.17: Comparison of peak frequency from TD and FD for both load conditions and motions.

Motion/LC	**Unit**	**FD ω_p**	**TD ω_p**	**Error**
Surge LC1	[rad/s]	0.000	0.038	-100.0 %
Surge LC2	[rad/s]	0.000	0.065	-100.0%
Pitch LC1	[rad/s]	0.157	0.000	NaN
Pitch LC2	[rad/s]	0.157	0.146	7.8%

Chapter 5

Discussion

The results that were presented gives rise to a discussion on their validity and on the relative performance compared towards SRA TD-simulations.

From the linear transfer functions it was clear that the force is inertia dominated, by comparison of the acceleration of the structure versus the excitation force. The natural frequency in heave was not included, which should be considered, as this represent a a maxima in the transfer function. The linear transfer functions can easily be a source to error, and from the figures that were presented, it was clear that there is no value obtained from the Wadam-analysis that represented when the frequency was zero. Consequently an extrapolation of these can yield to error early in the FD-method. These frequencies, that are very close to zero, have great influence on the contribution from the wind. Wind has large periods and most energy close to zero. From the figures of the wind spectra it was shown that the majority of energy is situated in an approximate range between 0-0.2 rad/s. This area contains the natural period in both surge and pitch, so it is important to consider if this can be a reason for error.

The plot of the mean drift forces showed peaks at the natural period in heave for heave-force and pitch-moment. Thus, comparing it to 1st order force, these forces are much smaller than the 1st order excitations. The force in surge motion at the towers 1st bending mode was rather large. This is situated away from the WF-region, so it would most likely

have to be excited by sum-frequency effects. Thus, this has not been examined in this thesis. In Kvittem and Moan [2014], this has been investigated. From a selection of representative tower base bending moment spectra presented there, it is clear that the first eigenmode of the turbine can have as great significance as the non-linear LF-part of the solution. Kvittem and Moan [2014] managed to capture some of the solution by use of a flexible model.

Examination of the peak frequencies in the force spectra show that the first order peaks shift towards left for an increasing severity of the sea-state. While the 2nd order force shifts towards right, or do not change at all. There are too few LC examined in order for this to be stated as a trend, however if it is, this substantiates that there are more 2nd order effects present, with increasing severity of the sea-state. This is due to that the 1st order forces, and 2nd order forces will overlap. Ergo, if the magnitude of the 2nd order force is substantial, it will cause large motions of the structure. Thus, the importance of including the slowly varying loads would be supported.

Evaluation of the motions spectrum for the three load-cases substantiates what was observed in the force-spectrum. That the peak frequency shifts towards left for WF-part and right for LF-part. Especially for the heave motion, the first order and second order effects are overlapping in all conditions. This indicates that the results obtained in LF-domain does not have any physical effect, and give reason to why the error in LF-domain become of significance for heave. The magnitude of the second order effect that is occurring in the WF-domain are relatively small, compared to the first order loads. It is also worth mentioning that in LC3, there is a peak rising in heave motion, which is not at all captured by the FD-results. For this case the shape shows little resemble between TD and FD. In addition, it is one of the few cases where the standard deviation in the WF-region is smaller for FD-result than the TD-result. The author do not have an explanation to why this occurs. Hence, it should give rise to questioning the validity in an extreme condition, and be further investigated.

The pitch-motion does not intersect between 1st order and 2nd order effects, but for LC3, its magnitude is much higher for the extreme sea-state. Moreover, the standard deviation

is almost the same in both frequency regions. This proves the importance of including the slowly varying loads in an extreme sea-state. The natural frequency in pitch has great influence in the LF domain, as the peaks are situated in close region to this for all LC that were investigated. Therefore, this should, in future application be included in the QTF in order to not underestimate the effect if this motion is excited.

The LF response in surge motion for the FD-solution propagates to a static value at the y-axis, for all LC that were examined. This is most likely due to that the QTF did not have a value for difference frequency of less than 0.1 rad/s, so this were extrapolated. In general one must be careful with extrapolation of data. For this case, there are too few data-points that follows the trend in this range. In addition, the TD-solution and the linear transfer function in surge yields that the curve should descend again somewhere in the area close to the natural frequency in surge. This was supposed to be implemented by imposing a frequency step for the Wadam analysis that were smaller than the natural period in surge. However, the sum of the frequencies should be less, and this was not covered when the first frequency is 0.5 rad/s. The author therefore recommends to either not apply the LF-motions spectrum for lower values than 0.1 rad/s or implement a better extrapolation, or run a modified analysis in Wadam.

When transferring the thrust force to its influence on the global motions of the hull, it is directly dependent on the linear transfer function for the relationship between external force and motion. As mentioned, the wind is most dominant at very low frequencies, and so it is questionable how well the motions can be represented where the transfer functions are extrapolated. For this purpose the linear transfer function in surge and pitch are applied, and from the figures that were presented it was clear that the last data-point has just started to descend from the peak. This gives a linear extrapolation based on only two points and can contribute to quite wrong results.

It should again be emphasized that the comparison between TD and FD-solution for the state-space model is based on only one TD-simulation, which at best can give a preliminary indication of verification of the FD-method. Since the active ballasting system has not been implemented in the FD-method, the simulation in SRA was also conducted without

ballasting. This should give the hull a mean offset in pitch motion, that causes the turbine to rotate. Consequently, the thrust-force should then experience a decrease compared to the behaviour with ballasting.

The logarithmic plot of the thrust force spectrum yielded that the peaks from the rotational multiples of the rotor are well represented. The magnitude were however rather small in comparison to the energy from the wind force for these load conditions. These frequencies are important as they can cause vibrations. If any comparison is to be made, Kvittem and Moan [2014] states that for for LC1 the frequency of the turbine is close to the eigenfrequency of the turbine, which substantiates the importance of including the effect of the rotor multiples.

There is definitely a possibility that personal error has occurred. Especially in the state-space model there was an enormous amount of data that was processed, and uncertainties regarding units and positions of the parameters that the model was condensed to. The author believes that this approach can yield good resemblance with further work, but it is advised to gain more control of the data. It was observed from the results, that for LC2 the pitch and surge motion is well represented for the higher frequencies in the spectra. This substantiates that there is error connected to the extrapolation. At least surge motion has poor tendencies, as all the peaks are at zero due to that the natural frequency in surge is note properly captured. For the parts in LC2 where the TD-spectrum and FD-spectrum follow the same trend, the FD-seems to be underestimated. This can be caused by that the damping is overestimated, but with this little data for comparison this will just be speculations. If it would have been a trend for several comparisons, the state-space model should be investigated to see if it is rigid enough.

For both motions, LC1 is poorly represented. The consequence is that the slightly better results in LC2 lose credibility, but the author believes that it must be an error in the script and that it should be possible to gain better results with the state-space model. It should be easier to represent the forces below rated wind speed than above rated wind speed. This is due to that the thrust force is quite linearly increasing below rated wind speed, while above rated wind speed the blades are pitched, trying to keep the torque constant.

The pitching of the blades influences the thrust force so that it has a non-linear descent with increase in wind speed.

Although it is not valid to state anything from comparison with one simulation, some parallel can be drawn to the work performed in Kvittem and Moan [2014]. Also in that work, there was struggle to recreate the wind induced motions in FD. As the author expected, the errors for the standard deviation in pitch motion tend to be smaller for LC1 than LC2, where the approximate error is roughly 10-20%. Thus, if the comparison done here is representable for a larger sample , it could give a better representation if the error that is most likely connected to extrapolation for LC2 is fixed, and if the error in LC1 is detected as bad programming.

Chapter 6

Conclusion

This thesis has focused on developing a frequency domain model for dynamic response analysis of the floating wind turbine, WindFloat. A literature review was conducted with focus on presenting various aspects to the benefits and disadvantages of frequency domain methods. Similar work was also summarized and later compared towards the results achieved in this thesis.

An outline on the theoretical background were presented. Procedure from time-domain to frequency-domain analysis, description of the dynamic problem and the necessary linearisation of the true problem were emphasized.

The hydrodynamic model was obtained by creating a mesh in GeniE, running Wadam analysis in HydroD and post-processing the results into spectral formulations of the linear and second order contributions to the dynamic equation of motion in the frequency domain. For validation, 10 seeds in SIMO-RIFLEX-AeroDyn (SRA) were averaged and compared.

The aerodynamic model was obtained by manipulation of a state-space model of an OC3 monopile. Through matrix manipulation the spectral formulations for the thrust force were obtained and transferred to the global coordinate-system for motion analysis.

Based on one below rated, one above rated and one extreme wind speed condition, most

probable wave height and peak period were selected as three loading conditions for investigation of the results.

The linear transfer functions obtained from Wadam, had to be extrapolated in the range 0 - 0.05 rad/s and the quadratic transfer functions representing the difference-frequency forces were extrapolated from 0-0.1 rad/s. This gave rise to uncertainties in the results that were acquired in this range that were dependent on either of the transfer functions.

With exception of errors up to 20% for standard deviation in LC3, the comparison to the solution obtained in SRA gave errors of less than 2.5%, for the estimated peak frequencies and standard deviations, in the wave frequency region for all load cases. In the low frequency region, surge motion experienced large errors for all load-cases due to poor extrapolation of the transfer functions that did not represent the true behaviour. The natural period in pitch was not included in the quadratic transfer function, which gave rise to large errors for estimated peak frequency at LC1, this effect did however descend for the following loading conditions.

For the results for the aerodynamic motion analysis the comparison towards SRA was only performed for one TD-simulation. Therefore, it is not possible to conclude on any of the results, as it is necessary to have a larger sample. However, what the results indicated will be summarized.

The comparison of the blade passing frequencies of the turbine showed less than 2.5% error for the loading conditions. When examining the motion spectra for the SSWT subjected to wind only, several uncertainties arose. LC1 experienced very bad comparison. LC2 showed that for frequencies larger than roughly 0.9 rad/s the FD-solution yielded good comparison to the TD-solution. In this load-case, pitch motion had the best representation with errors of less than 8%. These thoughts will just be speculation, and further investigation is advised.

The aerodynamic loads has the majority of the energy in the range where the transfer functions are extrapolated. This substantiates the importance of the linear transfer functions in this area. The aerodynamic method is not verified, but can be a good starting point

for further work. The results in the hydrodynamic frequency domain method in general yields good correspondence for LC1 and LC2 in all areas, if the extrapolated part is excluded. The second order forces has proven to be of significance, since both the pitch and surge natural frequency are excited in the LF domain. The method should be altered to the proposed improvements of the transfer functions, and further validated for more loading conditions for future application. In addition, superimposed wind and wave response should be evaluated.

Chapter 7

Recommendations for Further Work

Based on the results presented in the report and the knowledge gained in the process, the following suggestions are made for improvement and further development of the scientific field of FD-method for floating wind turbines.

Improvements

- From the results it is clear that the natural frequency in pitch has great influence on the dynamic response. By selecting a more sophisticated method of integration when calculating the second order force spectrum, this effect could be included. The numerical integration method must allow for the integration step to be variable.
- The exact heave natural frequency is not implemented, this has proven not to have as significant effect as the pitch natural frequency, it would however take small efforts to implement it for the linear transfer function by running an analysis in HydroD.
- The extrapolation of the QTF for surge in the area between 0.0 and 0.1 rad/s should be revised. It is certain that the line will intersect at the y-axis and not zero, a more dense frequency step about the range of 0.1 rad/s should give a more valid result for extrapolation. Until this is revised, frequencies below 0.1 rad/s should not be applied from the surge-motion spectrum.

Quality control

- As a starting point, the method should be validated for more load cases, at least for from cut-in to cut-out windspeed. Then also for a variety of sea-states. Different approaches to determining the load cases can be found in Li et al. [2015], where the joint probability with three variables should be considered for a fatigue analysis.
- The thrust force should be validated more properly towards TD-simulations. Attention should also be conducted to the moment in the tower base bending moment, to see if it coincides with transferring the thrust force from the rotor to the global coordinate system. There is little room for error in the stresses in a fatigue study, as fatigue damage is at minimum proportional to the stress-range to the power of three, accuracy is therefore important in the entire process.
- Validation of the wind-induced motion must be performed. It is probably an inherent error due to its dependence on the linear transfer function. Thus, the linear transfer function must be improved, and most likely an typing error in the code for LC1 must be detected. If the results are not satisfying the author would recommend to investigate the restoring stiffness from the mooring lines.

Further work

- Simulations with simultaneous wind and wave response by use of superposition should be evaluated. The method should then be validated towards TD-simulation and this will give a proper insight to the whether it is beneficial or not to have a combination of aerodynamic state-space model and a more conventionally obtained hydrodynamic model.
- The active ballasting system must be implemented into the model when analysing the simultaneous response from wind and wave. This is implemented in SRA by shifting of COG and altering the inertia of the turbine. This can be implemented into the mass matrix as variable dependent on mean wind speed.
- If the dynamic response analysis of the floating wind turbine shows satisfactory results the overall aim should be to establish a method for fatigue calculations in frequency domain, some of the methods proposed by Kühn [2001] could be an inter-

esting starting point for this work.

Bibliography

E. E. Bachynski. *Design and Dynamic Analysis of Tension Leg Platform Wind Turbines*. Ph.d.thesis, Norwegian University of Science and Technology, 2014.

E. E. Bachynski. Basic aerodynamics for wind turbines. lecture notes in tmr4505 integrated dynamic analysis of wind turbines, 2015a.

E. E. Bachynski. Course project. lecture notes in tmr4505 integrated dynamic analysis of wind turbines, 2015b.

E. E. Bachynski. Course project: Integrated dynamic analysis of wind turbines, 2015c.

E. E. Bachynski and T. Moan. Linear and nonlinear analysis of tension leg platform wind turbines. In *The Twenty-second International Offshore and Polar Engineering Conference*. International Society of Offshore and Polar Engineers, 2012.

E. E. Bachynski, V. Chabaud, and T. Sauder. Real-time hybrid model testing of floating wind turbines: sensitivity to limited actuation. *Energy Procedia*, 80:2–12, 2015.

P. Brodtkorb, P. Johannesson, G. Lindgren, I. Rychlik, J. Rydén, and E. Sjö. WAFO - a Matlab toolbox for the analysis of random waves and loads. In *Proc. 10'th Int. Offshore and Polar Eng. Conf., ISOPE, Seattle, USA*, volume 3, pages 343–350, 2000.

DNV. Sesam user manual, wadam, 2010.

DNV. Sesam user manual, hydrod, 2011.

DNV. Column-stabilised units. *No. DNV-RPC103*, page 20, 2012.

O. M. Faltinsen. *Sea loads on ships and offshore structures*, volume 1. Cambridge university press, 1993.

M. O. Hansen. *Aerodynamics of wind turbines*. Earthscan, UK, 2008. ISBN 978-1-84407-438-9.

B. J. Jonkman. *TurbSim user's guide: version 1.50*. National Renewable Energy Laboratory Golden, CO, USA, 2009.

J. M. Jonkman, S. Butterfield, W. Musial, and G. Scott. *Definition of a 5-MW reference wind turbine for offshore system development*. National Renewable Energy Laboratory Golden, CO, 2009.

M. J. Kühn. *Dynamics and design optimisation of offshore wind energy conversion systems*. Ph.d.thesis, TU Delft, Delft University of Technology, 2001.

M. I. Kvittem. *Modelling and response analysis for fatigue design of a semi-submersible wind turbine*. Ph.d.thesis, Norwegian University of Science and Technology, 2014.

M. I. Kvittem and T. Moan. Frequency versus time domain fatigue analysis of a semisubmersible wind turbine tower. *Journal of Offshore Mechanics and Arctic Engineering*, 137 (1):011901, 2014. ISSN 0892-7219. doi: 10.1115/1.4028340.

M. I. Kvittem and T. Moan. Time domain analysis procedures for fatigue assessment of a semi-submersible wind turbine. *Marine Structures*, 40:38–59, 2015. ISSN 0951-8339. doi: http://dx.doi.org/10.1016/j.marstruc.2014.10.009. URL `http://www.sciencedirect.com/science/article/pii/S0951833914000756`.

M. I. Kvittem, E. E. Bachynski, and T. Moan. Effects of hydrodynamic modelling in fully coupled simulations of a semi-submersible wind turbine. *Energy Procedia*, 24:351–362, 2012. ISSN 1876-6102.

L. Li, Z. Gao, and T. Moan. Joint distribution of environmental condition at five european offshore sites for design of combined wind and wave energy devices. *Journal of Offshore Mechanics and Arctic Engineering*, 137(3):031901, 2015. ISSN 0892-7219. doi: 10.1115/1.4029842.

MARINTEK. *RIFLEX theory manual*. 2012a.

MARINTEK. *SIMO theory manual Version 4.0 rev.1*. 2012b.

K. O. Merz. Environmental loads for frequency domain aeroelastic analysis of offshore wind turbines, 2015a.

K. O. Merz. A linear state-space model of an offshore wind turbine, implemented in the stas wind power plant analysis program, 2015b.

K. O. Merz, M. Muskulus, and G. Moe. A simple frequency-domain method for stress analysis of stall-regulated wind turbines. *Wind Energy*, 15(5):773–798, 2012.

A. S. Midling. Norskekysten krevende for bunnfaste vindturbiner til havs, November 2015. URL `http://petro.no/norskekysten-krevende-for-bunnfaste-vindturbiner-til-havs/32834`.

T. Moan. Nonlinear stochastic response analysis of marine structures., 2009.

P. J. Moriarty and A. C. Hansen. *AeroDyn theory manual*. National Renewable Energy Laboratory Golden, Colorado, USA, 2005.

A. Naess and T. Moan. *Stochastic Dynamics of Marine Structures*. Cambridge University Press, 2013.

D. Newland. *An introduction to random vibrations, spectral and wavelet analysis.*, volume 3rd edition. Essex, England: Longman Scientific & Technical, 1993.

J. Nilsen. Disse 11 problemene må løses om flytende havvind skal lykkes, November 2015. URL `http://www.tu.no/kraft/vindkraft/2015/11/04/disse-11-problemene-ma-loses-om-flytende-havvind-skal-lykkes`.

H. Ormberg and E. E. Bachynski. Global analysis of floating wind turbines: Code development, model sensitivity and benchmark study. In *The Twenty-second International Offshore and Polar Engineering Conference*, pages 366–373. International Society of Offshore and Polar Engineers, 2012.

R. J. Ros and M. Costa. Floating offshore wind: Market and technology review, 2015. URL http://www.carbontrust.com/media/670664/floating-offshore-wind-market-technology-review.pdf.

D. Snieckus. Floating array of portugal by 2018, 2015. URL http://www.ewea.org/annual2015/wp-content/uploads/EWEA-2015-day-one.pdf.

J. Van Der Tempel. *Design of support structures for offshore wind turbines*. Ph.d.thesis, TU Delft, Delft University of Technology, 2006.

E. N. Wayman, P. Sclavounos, S. Butterfield, J. Jonkman, and W. Musial. Coupled dynamic modeling of floating wind turbine systems. Offshore Technology Conference, 2006. ISBN 155563253X.

Appendix A

Description of the Content in the Attached Zip-file

This appendix will give a brief description to the content in the attached Zip-file of the master thesis. The zip-file includes the different models from the software that is used and MATLAB code. In addition, the poster that was submitted for the mandatory master thesis poster exhibition is appended. This appendix will give a brief description of the folder hierarchy.

MATLAB

The post-processing in MATLAB is organized as follows.

Environment

Output JONSWAP spectra for the different load conditions. Environment file also includes the description of the different distributions from Li et al. [2015] although this has not been implemented in the thesis. It is a possible starting point to calculate the probability of occurrence for each sea-state for fatigue analysis.

Main Hydrodynamic

Initiated by run_hydrodynamic.m Connects a lot of the work performed in the other scripts.

Main Aerodynamic

The shell of the main script is a shell provided by Karl Merz. Partitions the matrices in the state space model to output the spectra for the turbine forces. Calculates the eigenvalue problem for a range of frequencies. This script require more input to run. Due to the limitations of the size of the zipped folder this is not attached.

Postprocess SRA

In postprocess SRA: findinflections, readTimeDomainResults and replaceinfile is provided by Erin E. Bachynski.

Calculates the averaged standard deviations and peak periods.

Create Input Files

Code for rewriting the QTF from Wadam to SRA, and for altering the inpmod-file in SRA to increase elastic modulus.

SRA

Input files for wind-only configuration and wave-only configuration is appended. The QTF is included. A brief description is given below.

- sys-WFloat.dat: Is the SIMO system file. Includes the mass coefficients and COG, added mass-, linear stiffness- , linear damping- and quadratic damping-matrix. Linear transfer functions, quadratic transfer functions and retardation functions.

- WFloat_inpmod.inp: RIFLEX input file. Includes environment data, description on whether blades are pitched or not, identify the beam-representation on slender elements, with supernodes and whether they are free, fixed or a master-slave connection.
- WFloat_dynmod.inp: RIFLEX input file for dynamic analysis. Includes information on simulation length and time-step for calculation
- ad_dll_inputs.txt: Information on what to output, and constant wind.
- aerodyn.ipt : information on which wind-input file to use, whether to use BEM or GDW, type of dynamic stall etc. In addition to position of airfoil data.
- WFloat_outmod.inp: Information to output the frequencies from the wave-loads.

GeniE

Contains the model in GeniE. This model can be re-meshed for application in HydroD.

- js. files. Environment in GeniE

HydroD

Everything that is necessary to run new simulations in hydroD is appended.

- newsemi2.hyd : Environment in HydroD
- js. files: Javascript files in HydroD.
- byT1.FEM: file for structure from GeniE.
- fsT1.FEM: file for second order free surface from GeniE.
- T2.FEM file for Morison model from Marit L. Kvittem.
- G1.sif Result file from one simulation.